Molecular Therapy
Original Article

Functional screening identifies miRNAs with a novel function inhibiting vascular smooth muscle cell proliferation

Julie Rodor,[1] Eftychia Klimi,[1] Simon D. Brown,[1] Georgios Krilis,[1] Luca Braga,[2] Nadja A.R. Ring,[2] Margaret D. Ballantyne,[1] Despoina Kesidou,[1] Aurelie Nguyen Dinh Cat,[1] Vladislav Miscianinov,[1] Francesca Vacante,[1] Katarina Miteva,[1] Matthew Bennett,[1] Abdelaziz Beqqali,[1] Mauro Giacca,[3,4] Serena Zacchigna,[2,4] and Andrew H. Baker[1,5]

[1]Centre for Cardiovascular Science, The Queen's Medical Research Institute, University of Edinburgh, EH16 4TJ Edinburgh, UK; [2]International Centre for Genetic Engineering and Biotechnology (ICGEB), 34149 Trieste, Italy; [3]British Heart Foundation Centre of Research Excellence, School of Cardiovascular Medicine & Sciences, King's College London, SE5 9NU London, UK; [4]Department of Medical, Surgical and Health Sciences, University of Trieste, 34129 Trieste, Italy; [5]CARIM School for Cardiovascular Sciences, Department of Pathology, Maastricht University Medical Center (MUMC), 6229HX Maastricht, the Netherlands

Proliferation of vascular smooth muscle cells (vSMCs) is a crucial contributor to pathological vascular remodeling. MicroRNAs (miRNAs) are powerful gene regulators and attractive therapeutic agents. Here, we aimed to systematically identify and characterize miRNAs with therapeutic potential in targeting vSMC proliferation. Using high-throughput screening, we assessed the impact of 2,042 human miRNA mimics on vSMC proliferation and identified seven miRNAs with novel vSMC anti-proliferative function: miR-323a-3p, miR-449b-5p, miR-491-3p, miR-892b, miR-1827, miR-4774-3p, and miR-5681b. miRNA-mimic treatment affects proliferation of vSMCs from different vascular beds. Focusing on vein graft failure, where miRNA-based therapeutics can be applied to the graft *ex vivo*, we showed that these miRNAs reduced human saphenous vein smooth muscle cell (HSVSMC) proliferation without toxic effect. HSVSMC transcriptomics revealed a distinct set of targets for each miRNA, leading to the common downregulation of a cell-cycle gene network for all miRNAs. For miR-449b-5p, we showed that its candidate target, *CCND1*, contributes to HSVSMC proliferation. In contrast to HSVSMCs, miRNA overexpression in endothelial cells led to a limited response in terms of proliferation and transcriptomics. In an *ex vivo* vein organ model, overexpression of miR-323a-3p and miR-449b-5p reduced medial proliferation. Collectively, the results of our study show the therapeutic potential of seven miRNAs to target pathological vascular remodeling.

INTRODUCTION

Vascular remodeling is an essential process of adaptive structural change in the vessel wall. It involves changes in vascular wall thickness, which confer elevated vascular resistance in response to pathological, hemodynamic, or iatrogenic injurious cues. However, this process can become aberrant, resulting in the development of vascular pathologies such as atherosclerosis and pulmonary hypertension[1] as well as the intimal hyperplasia underlying saphenous vein graft failure.[2]

Integral to the etiology of the vascular remodeling process is the switch of resident vascular smooth muscle cells (vSMCs) from a differentiated and quiescent to a de-differentiated, pro-proliferative and pro-migratory phenotype.[3,4] On the molecular level, excessive proliferation of vSMCs is a complex process linked to injury of the endothelial cell (EC) layer and the subsequent inflammatory response.[5] The platelet-derived growth factor (PDGF) has been shown to play a crucial role in vSMC response,[5] and activation of PDGF-BB in combination with the interleukin-1α (IL-1α) pathway has been shown to promote proliferation *in vitro* in human saphenous vein smooth muscle cells (HSVSMCs).[6]

Targeting vSMC proliferation is thus an attractive therapeutic strategy for preventing adverse vascular remodeling in response to injury. Approaches based on reducing vSMC proliferation have been successful pre-clinically and have shown promising clinical results, as demonstrated by animal studies and clinical trials testing the use of anti-proliferative pharmacological agents in drug-eluting stents used for coronary angioplasty.[7] The pitfall of these approaches, however, has been interference with re-endothelialization, a process integral to countering the subsequent pathological vascular remodeling events that are initiated following EC injury and denudation.[7,8] In the case of vein graft failure, therapy based on gene transfer has been considered and developed due to *ex vivo* access to the graft at the time of surgery.[9,10]

Received 17 January 2024; accepted 27 December 2024;
https://doi.org/10.1016/j.ymthe.2024.12.037.

Correspondence: Andrew H. Baker, Centre for Cardiovascular Science, The Queen's Medical Research Institute, University of Edinburgh, EH16 4TJ Edinburgh, UK.
E-mail: andy.baker@ed.ac.uk

MicroRNAs (miRNAs) are small non-coding RNA molecules (20–24 nucleotides in length) that regulate gene expression through imperfect base pairing with regions in the 3′ UTR of target messenger RNAs (mRNAs), inducing their degradation or translational repression.[11] miRNAs have been shown to play critical roles in a range of biological contexts, including development, cancer, and neurodegenerative disease.[12] In cardiovascular physiology, dysregulation of several miRNAs has been implicated in the development of multiple diseases.[13] For example, the smooth muscle cell (SMC)-enriched miR-143/145 cluster has been involved in vascular remodeling across several diseases, such as neointimal lesion formation, pulmonary arterial hypertension, and atherosclerosis.[14] Multiple miRNAs regulating vSMC phenotypes[15] and, more particularly, vSMC proliferation[16] have also been reported.

Due to their potent effect in regulating multiple gene expression changes, miRNA-based therapeutic approaches have been developed in multiple disease contexts, including cardiovascular disease, with ongoing clinical trials.[17,18] These approaches rely on the ability to modulate miRNA abundance using miRNA mimics, inhibitors, or viral-vector-mediated overexpression of an miRNA locus. To select the best miRNA candidates for therapy in an unbiased way, functional screens have been developed. In particular, microscopy-based screens have been used successfully, initially using hundreds of miRNAs and more recently using a library of 2,042 miRNAs covering all miRNAs present in the miRBase database.[19] In the cardiovascular field, miRNAs regulating cardiomyocyte proliferation have been identified using a microscopy-based screen,[20] and further testing showed that one of them, miR-199a, stimulates cardiac regeneration *in vivo* in mouse[20] and also in pig.[21] Therefore, miRNA-based therapy could be used to target aberrant vSMC proliferation in different diseases. In vein graft failure, while direct treatment of the graft with miRNA mimics or inhibitors could be achieved, a gene therapy strategy overexpressing miRNAs might be more effective and provide better control of expression.[10]

Here, we implemented an miRNA high-content imaging screen to identify miRNAs blocking vSMC proliferation. Seven miRNAs with an anti-proliferative effect across SMCs from different vascular beds were identified and further studied in the context of vein graft failure. In saphenous vein SMCs, we confirmed a strong decrease in proliferation, with no detrimental effect, upon overexpression of the seven miRNAs. Transcriptomics analysis combined with miRNA target prediction showed distinct targets for the seven miRNAs, leading to a common regulation of a network of core cell-cycle genes. In contrast, we observed limited proliferation and transcriptomics changes in saphenous vein ECs after miRNA overexpression. Importantly, we showed the therapeutic potential of miR-323a-3p and miR-449b-5p in an *ex vivo* vein organ model.

RESULTS

Functional screening identifies miRNAs that block vSMC proliferation

To identify miRNAs exerting an anti-proliferative phenotype in vSMCs upon exogenous expression in an unbiased manner, we performed a high-throughput high-content miRNA screening in human pulmonary artery SMCs (HPASMCs) using a library of miRNA mimics corresponding to 2,042 unique human mature miRNA sequences (Figure 1A). miRNA mimics were transfected at a concentration of 50 nM, and after 48 h, 5-ethynyl-2′-deoxyuridine (EdU) was added to assess the effect on HPASMC proliferation. High-content fluorescence image analysis was used to quantify viable (Hoechst 33342+) and proliferating (EdU+/Hoechst 33342+) HPASMCs. The screen included the overexpression of four different miRNA controls (miR-CTRLs), and the effect on proliferation was assessed relative to the average of the four miR-CTRLs (Table S1).

Twenty-two miRNAs with a large decrease on cell count (Hoechst 33342+) were discarded from our analysis due to likely toxicity (Figure 1B). Based on a 2-fold change in the percentage of EdU+ cells relative to the four miR-CTRLs, we identified 715 miRNAs with an anti-proliferative effect and 417 miRNAs with a pro-proliferative effect in HPASMCs (Figure 1B and Table S1). The lists of pro- and anti-proliferative miRNAs included several miRNAs with known effects on vSMC proliferation,[16] providing confidence in the screen result validity. Indeed, the known pro-proliferative miRNAs miR-146a and miR29a had a positive effect on HPASMC proliferation in the screen assay, while the known anti-proliferative miRNAs miR-124, miR-214, and miR-34a showed a decrease in HPASMC proliferation (Figure S1).

Ten miRNAs had a strong effect on HPASMC proliferation, reducing the number of EdU+ nuclei to 0 without a marked reduction in cell count (Table S1). The list of 10 miRNAs included miR-34a-3p, a known anti-proliferative miRNA mentioned above. We selected seven miRNAs for further study based on novelty in the cardiovascular field: miR-323a-3p (Figure 1C), miR-449b-5p, miR-491-3p, miR-892b, miR-1827, miR-4774-3p, and miR-5681b (Figure S2).

The effect of mimic-mediated overexpression of these seven miRNAs on HPASMC proliferation was confirmed on four additional biological replicates (Figure 1D). We also tested the effect of miRNA overexpression on SMCs from different vascular beds using the same conditions and technology as the screen. All seven miRNA candidates showed a significant reduction in EdU incorporation in human coronary artery SMCs (HCASMCs) (Figure 1E). In human umbilical vein SMCs (HUVSMCs), six of the seven miRNAs (miR-323a-3p, miR-449b-5p, miR-491-3p, miR-892b, miR-1827, and miR-4774-3p) showed a significant decrease in the percentage of EdU+ cells (Figure 1F).

These data suggest that the overexpression of these seven miRNAs could have the therapeutic potential to reduce vSMC proliferation across different vascular pathologies.

Overexpression of miRNA candidates reduces proliferation and migration of HSVSMCs without any toxic effect

As SMC proliferation contributes to pathological remodeling in vein graft failure and therapeutic intervention can be implemented *ex vivo*

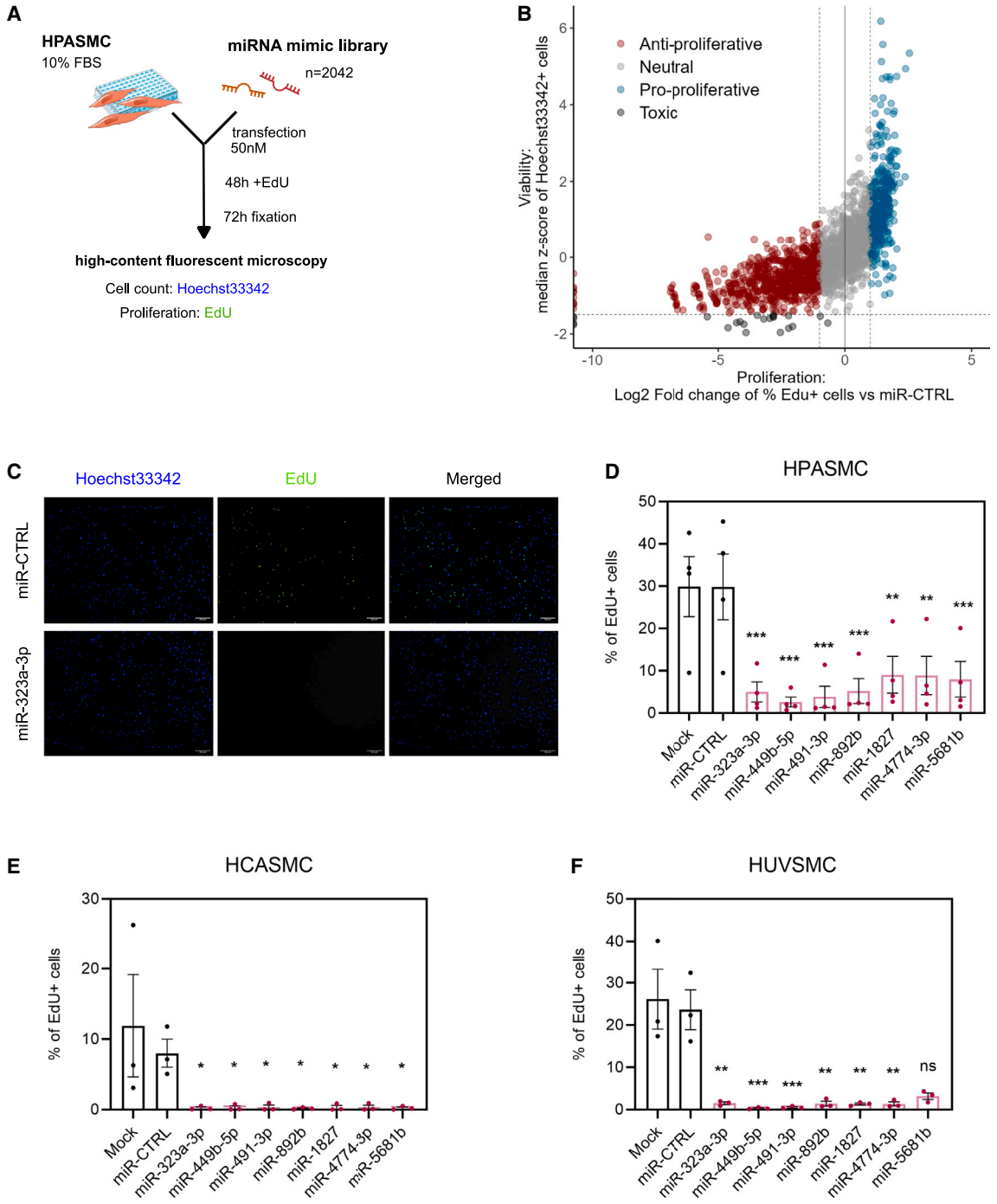

Figure 1. High-throughput miRNA screen identifies novel miRNAs regulating vSMC proliferation

(A) Schematic of high-throughput miRNA screen design in vSMCs. (B) Scatterplot of viability (expressed as median *Z* score of Hoechst 33342+ cells) and proliferation (expressed as log2 fold change of %EdU+ cells versus miR-CTRL) changes for each mimic-mediated miRNA overexpression ($n = 1$). (C) Representative images of HPASMCs stained with Hoechst 33342 (blue) and EdU (green) following treatment with miR-323a-3p mimic and miR-CTRL. Scale bars, 200 μm. (D–F) Percentage of EdU+ cells based on high-throughput microscopy imaging quantification in (D) HPASMCs ($n = 4$), (E) HCASMCs ($n = 3$), and (F) HUVSMCs ($n = 3$) transfected with seven candidate miRNA mimics or miR-CTRL, as well as the "mock" transfection control (lipofectamine-treated cells). Statistical analyses were performed using Iman and Conover non-parametric ranking followed by a repeated-measures ANOVA, and the *p* value was calculated for the comparison between miRNA-mimic treatment and miR-CTRL using Dunnett's test for multiple comparisons. On the graphs, error bars correspond to standard error of the mean and $^{*}p < 0.05$, $^{**}p < 0.01$, and $^{***}p < 0.001$, and ns, non-significant. *n* corresponds to distinct biological replicates.

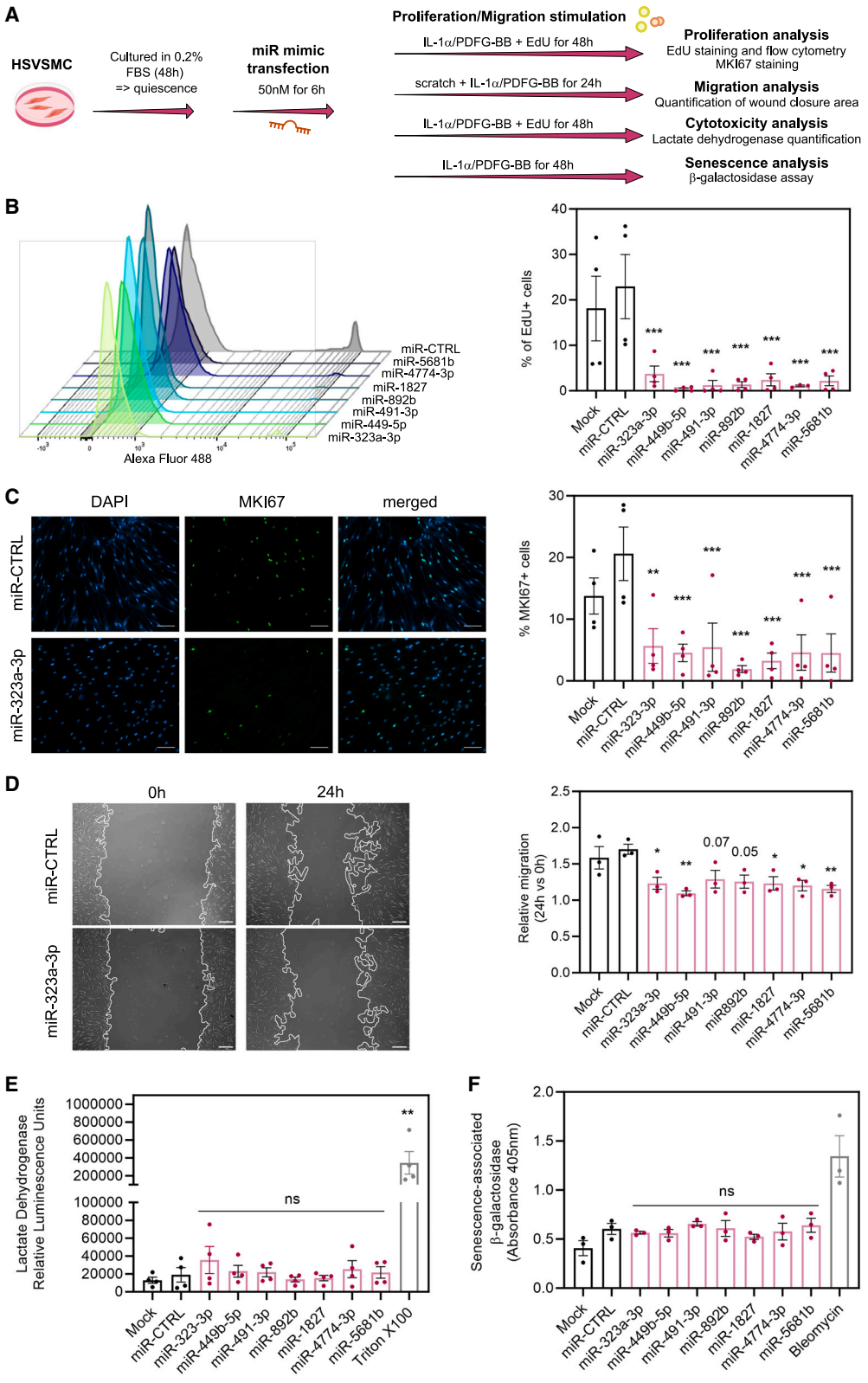

(legend on next page)

at the time of grafting, miRNA-based therapy could be a suitable strategy for this pathology. Hence, we investigated further the expression and effect of the seven miRNAs in primary HSVSMCs. We performed mimic-mediated overexpression of the seven miRNAs in HSVSMCs, and phenotypic switching (de-differentiated, pro-proliferative, and pro-migratory phenotype) was induced using a combination of IL-1α and PDGF-BB (Figure 2A), as this co-stimulation has been previously shown to promote a strong proliferative response in HSVSMCs.[6] We assessed the effect of the miRNA overexpression on proliferation and migration but also checked for any potential detrimental effect by analyzing cytotoxicity, apoptosis, and senescence.

Overexpression of the seven miRNAs was confirmed by reverse transcription (RT)-qPCR (Figure S3). It was noted that all seven miRNAs have low or no endogenous expression (based on qPCR cycle threshold value; data not shown) in quiescent and IL-1α/PDGF-BB-treated HSVSMCs, suggesting that any phenotype observed in mimic-treated HSVSMCs will be linked to their exogenous expression. Flow cytometric quantification of EdU incorporation in HSVSMCs showed significant decreases in IL-1α/PDGF-BB-induced proliferation (decrease ranging from 83.7% to 98.2%) after transfection with the seven miRNA mimics compared to miR-CTRL (Figure 2B). This decrease in proliferation was confirmed by MKI67 staining (Figures 2C and S4). We also observed that five of the seven miRNAs significantly reduced the migration rate of IL-1α/PDGF-BB-stimulated HSVSMCs, assessed by scratch wound assay (Figures 2D and S5). We did not detect any toxic effect upon miRNA overexpression, based on lactate dehydrogenase cytotoxicity assay (Figure 2E) and caspase-3 activity assay (Figure S6). Furthermore, no significant change in senescence, measured by senescence-associated (SA) β-galactosidase activity, was observed following overexpression of the seven miRNAs (Figure 2F).

While we observed a strong decrease in proliferation with no associated toxic effect in HSVSMCs using a 50 nM concentration of mimics for the candidate miRNAs, we also performed a dose-dependent experiment to see if the proliferation phenotype could still be observed with a lower dose of mimics. We observed a significant overexpression of all candidate miRNAs with a 10 nM mimic concentration and a significant increase for six of the seven miRNAs using a low concentration of mimics of 2 nM (Figure S7). Interestingly, we observed a significant downregulation of *MKI67* expression by RT-qPCR with all doses of mimics (Figure S8), showing that a decrease in proliferation could be achieved at low concentration of mimics.

These results demonstrate that overexpression of the candidate miRNAs reduces IL-1α/PDGF-BB-induced HSVSMC proliferation and migration without causing HSVSMC cytotoxicity, apoptosis, nor senescence, making them good candidates for therapy in the vein graft failure context.

Transcriptome analysis revealed the regulation of a common network of cell-cycle genes by all seven miRNAs

To understand the effect of the miRNA overexpression at the transcriptomic level, we performed RNA sequencing (RNA-seq) on quiescent HSVSMCs and IL-1α/PDGF-BB-induced HSVSMCs treated with the different miRNA mimics. The principal-component analysis (PCA) showed distinct clusters based on condition and patient origin of the HSVSMCs (Figure S9). As expected, IL-1α/PDGF-BB-induced HSVSMCs clustered separate from quiescent cells. After removal of batch/patient effect, the PCA clearly showed that all of the miRNA-treated samples did not overlap with their relative IL-1α/PDGF-BB controls (no treatment, mock treatment, or miR-CTRL) and were also distinct from quiescent cells (Figure 3A). This revealed that miRNA overexpression affects the transcriptome but does not revert it to a "quiescent cell" transcriptome. We performed a differential expression analysis between each miRNA mimic overexpression condition and miR-CTRL condition. As we observed sample separation based on patient origin in the PCA plot, we corrected for patient variance in the differential gene expression analysis. Based on a 2-fold change threshold, we detected between 393 and 1,013 differentially expressed genes associated with the miRNA overexpression (changes for miR-323a-3p shown in Figure 3B and all other changes in

Figure 2. The overexpression of seven candidate miRNAs affects HSVSMC proliferation and migration *in vitro*

(A) Schematic of the experimental design for assessing the effect of miRNA overexpression on IL-1α/PDGF-BB-treated HSVSMCs. (B) Flow cytometric quantification of EdU incorporation in IL-1α/PDGF-BB-stimulated HSVSMCs transfected with the seven miRNA mimics versus miR-CTRL and lipofectamine-treated cells (mock). On the left, representative EdU plot, and on the right, bar graph quantification ($n = 4$, except $n = 3$ for miR-4774-3p). Statistical analyses were done using a mixed-effects model. (C) Percentage of MKI67-positive cells in IL-1α/PDGF-BB-stimulated HSVSMCs transfected with the seven miRNA mimics or miR-CTRL, as well as the mock transfection control ($n = 4$). On the left, representative images (DAPI, EdU, and combined) for miR-CTRL and miR-323a-3p (scale bars, 100 μm). On the right, bar graph quantification. Statistical analyses were done using Iman-Conover non-parametric ranking followed by repeated-measures ANOVA. (D) Wound healing assay of IL-1α/PDGF-BB-stimulated HSVSMCs transfected with the seven miRNA mimics or miR-CTRL, as well as the mock transfection control. On the left, representative images from the scratch assay at 0 and 24 h for miR-CTRL and miR-323a-3p. Scale bars, 500 μm. On the right, quantification of wound healing (24 h area versus 0 h area) via the ImageJ MRI wound healing tool ($n = 3$). Statistical analyses were done using Iman-Conover non-parametric ranking followed by repeated-measures ANOVA. (E) Lactate dehydrogenase activity in IL-1α/PDGF-BB-stimulated HSVSMCs transfected with the seven miRNA mimics or miR-CTRL, as well as the mock transfection control ($n = 4$). HSVSMCs treated with Triton X-100 were used as a positive control for cytotoxicity induction. Statistical analyses were done using Iman-Conover non-parametric ranking followed by repeated-measures ANOVA. (F) Quantification of senescence-associated (SA) β-galactosidase activity (absorbance measured at 405 nm) in IL-1α/PDGF-BB-stimulated HSVSMCs transfected with the seven miRNA mimics or miR-CTRL, as well as the mock transfection control ($n = 3$). Bleomycin (1 μg/mL) was used as a positive control for senescence induction. Statistical analyses were done using Iman-Conover non-parametric ranking followed by repeated-measures ANOVA. p values for the comparison between miRNA-mimic treatment and miR-CTRL treatment obtained after Dunnett's test for multiple corrections are included on the graphs: $^{*}p < 0.05$, $^{**}p < 0.01$, $^{***}p < 0.001$, and ns, non-significant. Error bars correspond to standard error of the mean. n corresponds to distinct biological replicates.

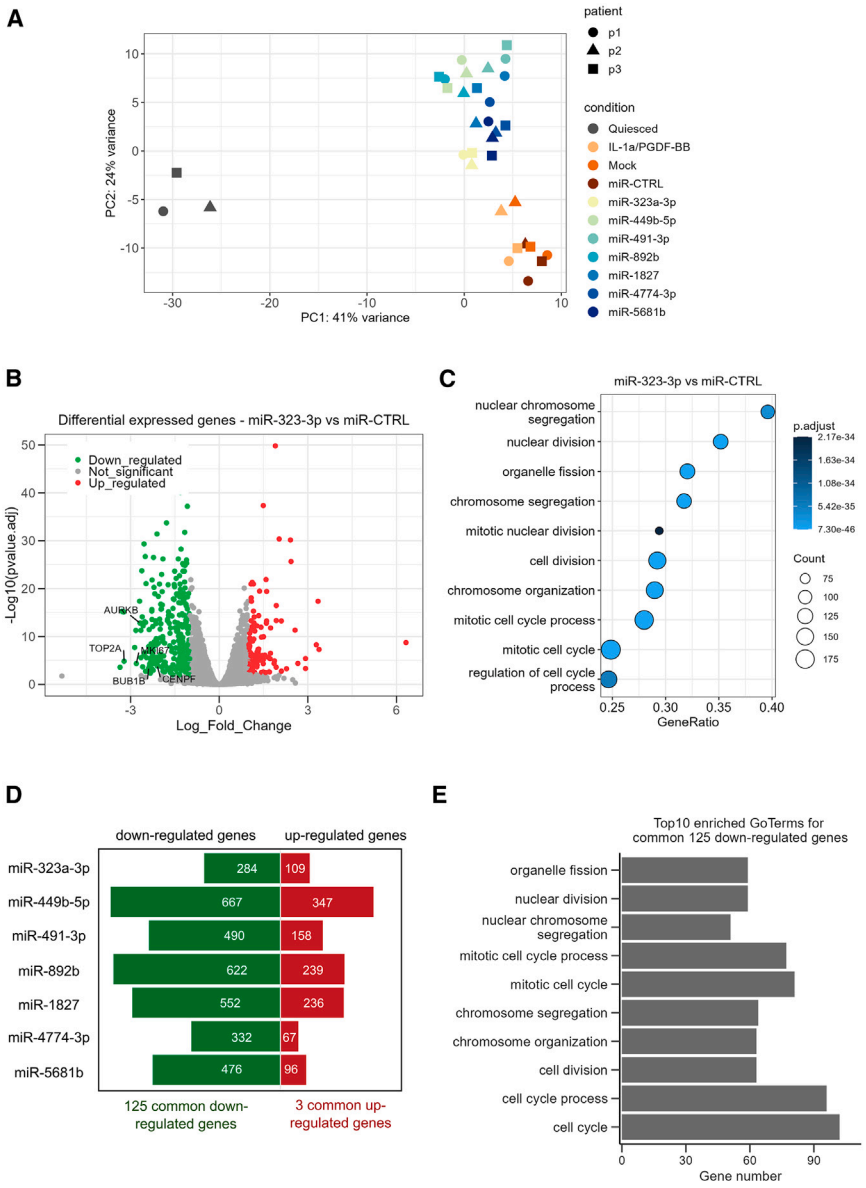

Figure 3. Transcriptomic changes upon overexpression of the seven candidate miRNAs in HSVSMCs

(A) Principal component analysis plot of HSVSMC RNA-seq after removal of batch effect (removal of patient effect). (B) Volcano plot showing the fold change and *p* value for all expressed genes for the comparison of miR-323a-3p mimic versus miR-CTRL (based on DESeq2 analysis with *p* values obtained using the Wald test followed by the Benjamini and Hochberg method for multiple correction). Significant changes were identified using a threshold of absolute fold change ≥ 2 and adjusted $p < 0.01$. Cell-cycle genes *MKI67*, *TOP2A*, *BUB1B*, *AURKB*, and *CENPF* are highlighted. (C) Top 10 enriched GO terms (biological process) for genes differentially expressed upon miR-323a-3p overexpression based on gene set enrichment analysis. (D) Number of significantly differentially expressed genes for each miRNA overexpression versus miR-CTRL based on an absolute fold change ≥ 2, adjusted $p = 0.01$, and minimum expression of 2 FPKM in at least two of the miR-CTRL/miR-mimic samples. The number of genes commonly regulated by all miRNAs is indicated below. (E) Top 10 enriched GO terms (biological process) for the 125 genes commonly downregulated by all seven miRNAs.

Figure S10; a list of differentially expressed genes is included in Table S2). As expected, based on the anti-proliferative phenotype, we observed the downregulation of known cell-cycle genes such as *MKI67*, *TOP2A*, *BUB1B*, *AURKB*, and *CENPF* upon each miRNA overexpression (Figures 3B and S10). A gene set enrichment analysis using each list of differentially expressed genes revealed that the top enriched Gene Ontology (GO) terms for all the miRNAs' overexpression were exclusively related to cell-cycle process (Figures 3C and S11 and Table S3) This is in agreement with the strong effect of miRNA overexpression on HSVSMC proliferation and showed that similar pathways are regulated by the seven miRNAs. As some of the miRNA overexpression also led to a migratory phenotype, we screened the list of enriched GO terms and found migration-related GO terms for miR-323a-3p, miR-449b-5p, miR-491-3p, miR-892b, miR-1827, and miR-5681b (Table S3). As the regulation of similar pathways by the seven miRNAs might correspond to the regulation of similar genes, we assessed the overlap of the differentially regulated genes and identified 3 genes commonly upregulated and 125 genes commonly downregulated by all seven candidate miRNAs (Figure 3D). Interestingly, the enriched GO terms of the 125 downregulated genes were related to cell-cycle process (Figure 3E). We found 102 of the 125 downregulated genes associated with the "cell cycle" GO terms annotation (Figure S12), and 17 of them were associated with the KEGG cell-cycle pathway, which includes the main components required for mitotic cell-cycle progression (Figure S13). This analysis suggests the anti-proliferative phenotype is mediated by the regulation of the same core cell-cycle genes and cell-cycle regulators for all seven miRNAs.

The mechanism of action of the seven miRNAs involved distinct targets

To characterize the mechanism of action of each miRNA, we aimed to identify their direct targets in proliferating HSVSMCs. As miRNAs are negative post-transcriptional regulators of gene expression, we focused our analysis on downregulated genes upon miRNA overexpression and used prediction tools to identify potential miRNA-

A

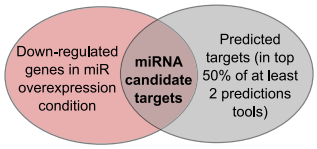

B

miRNA	Down-regulated Genes	Predicted targets	Candidate targets
miR-323a-3p	284	4199	**92**
miR-449b-5p	666	4327	**176**
miR-491-3p	490	2624	**96**
miR-892b	622	3955	**149**
miR-1827	552	6214	**224**
miR-4774-3p	332	1160	**15**
miR-5681b	476	983	**13**
	Total unique targets:		**680**

C

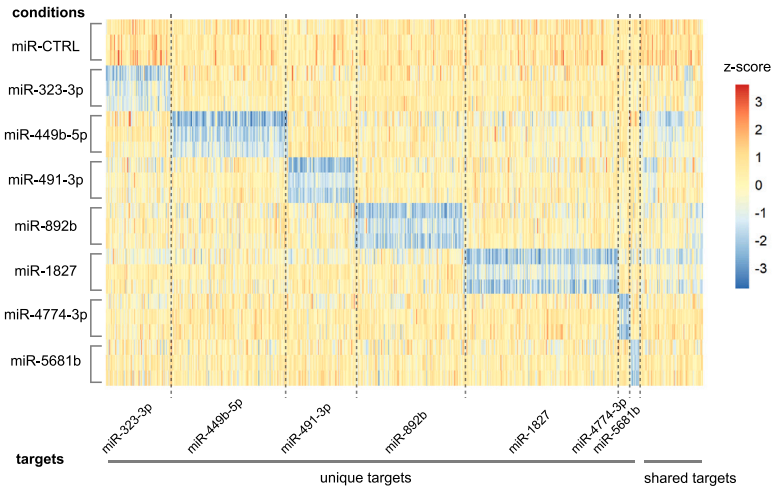

D

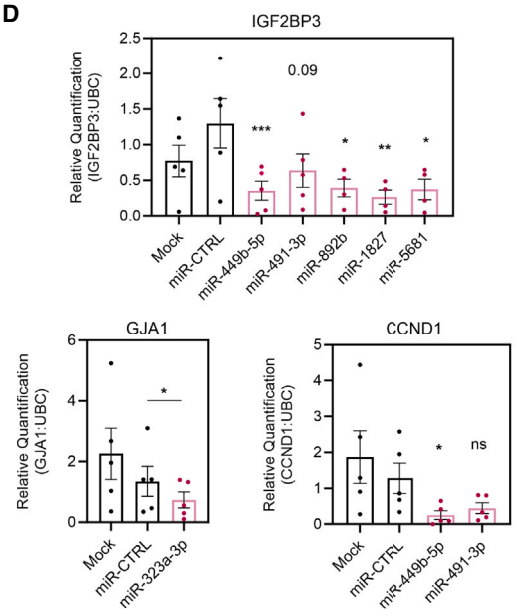

E

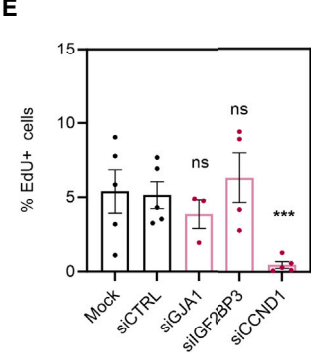

Figure 4. The seven candidate miRNAs regulate distinct targets in HSVSMCs

(A) Approach to identify miRNA targets based on down-regulation in RNA-seq upon mimic treatment and a combination of prediction tools. (B) Number of downregulated genes, predicted targets, and candidate targets for each miRNA. (C) Heatmap (expression displayed as column *Z* score of log2(FPKM + 1)) of all candidate targets for the seven miRNAs in the HSVSMC RNA-seq with a separation between unique and shared targets. (D) Validation of candidate target *IGF2BP3* (n = 4–5), *GJA1* (n = 5), and *CCND1* (n = 5) expression changes upon miRNA overexpression by RT-qPCR. Statistical analyses were done using a mixed-effects model for *IGF2BP3* and a repeated-measures ANOVA for *GJA1* and *CCND1*. p values for the comparison between miRNA-mimic treatment and miR-CTRL treatment obtained after Dunnett's test for multiple corrections are included on the graphs: $^{*}p < 0.05$, $^{**}p < 0.01$, $^{***}p < 0.001$, and ns, non-significant. (E) Percentage of EdU-positive HSVSMCs upon siRNA-mediated candidate target knockdown (n = 3–5). Statistical analyses were done using a mixed-effects model. p values for the comparison between each target knockdown treatment and siRNA control (siCTRL) treatment obtained after Dunnett's test for multiple corrections are included on the graph: $^{***}p < 0.001$ and ns, non-significant. Error bars correspond to standard error of the mean. n corresponds to distinct biological replicates.

mRNA interactions (Figure 4A). We used multimiR, a prediction tool package that compiles several target prediction algorithms,[22] and kept predicted targets ranked in the top 50% of at least two prediction tools. We identified between 13 and 224 candidate targets for the different miRNAs (Figure 4B and Table S4), with a total of 680 candidate targets if we consider all seven miRNAs together. Of the identified 680 targets, 89.4% are unique to one specific miRNA, while only 72 genes (10.6%) were candidate targets for at least two miRNAs (Figure 4C). We did not identify any gene targeted by all seven miRNAs but revealed that *IGF2BP3* could be targeted by five of the seven miRNAs. These data suggest that each miRNA has a distinct mechanism of action. Interestingly, miR-323a-3p, miR-449b-5p, miR-892b, and miR-1827 can directly target some of the 125 common downregulated genes, suggesting a possible direct mechanism on this network, while the regulation of the network by the other miRNAs might be indirect. Then, we assessed if any of the seven miRNA candidate target genes could be involved in the process, progression, and/or regulation of the cell cycle using the GO term annotation "cell cycle." We found that six of the seven miRNAs have at least one target gene related to "cell cycle," though these are still mostly different candidate targets per miRNA (Figure S14).

We also performed GO terms analysis of the miRNA candidate targets. miR-4774-3p and miR-5681b were not included in this analysis, as their numbers of candidate targets are too low (15 and 13 candidates, respectively). We found cell-cycle enriched GO terms only

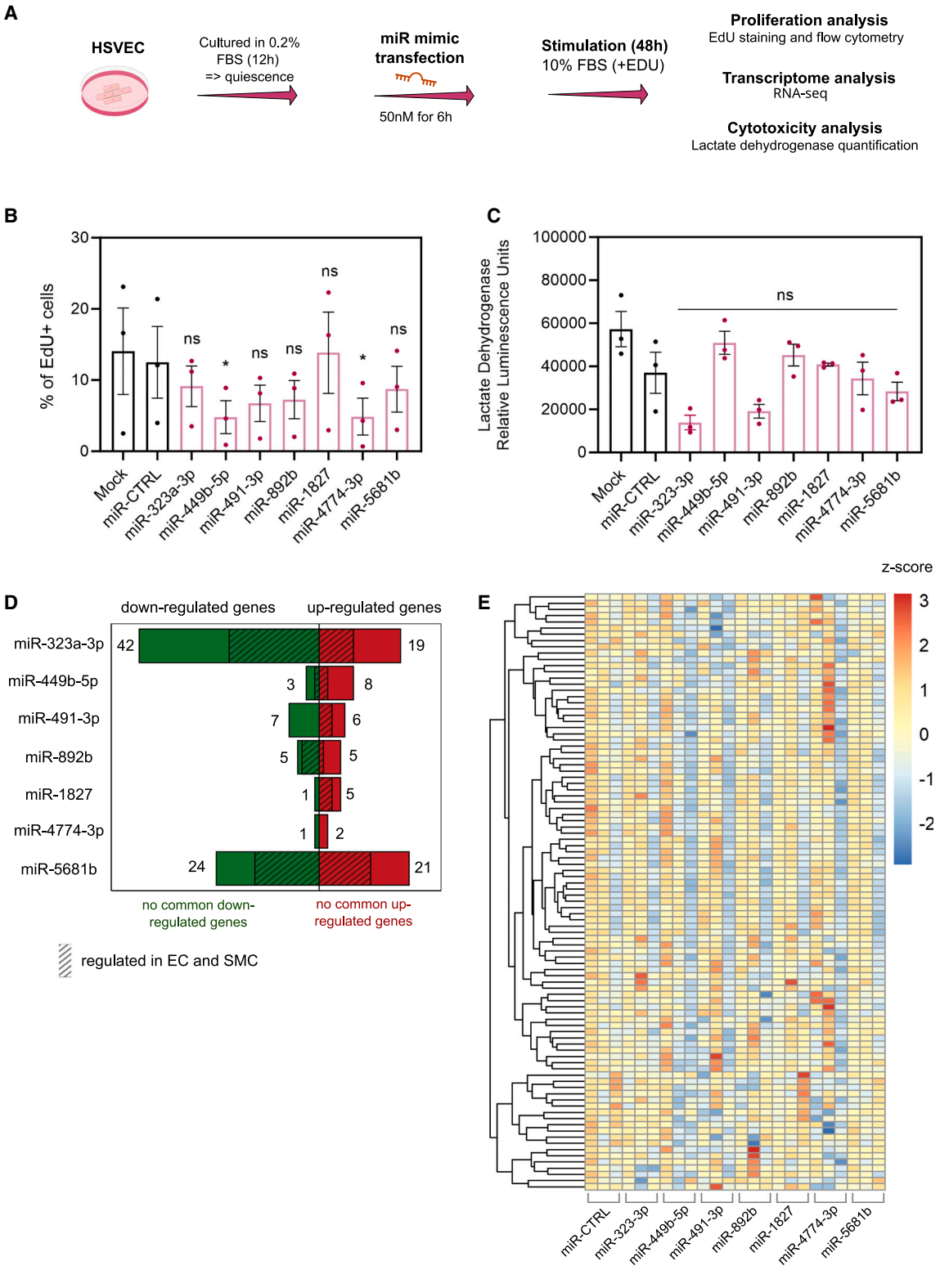

(legend on next page)

for the targets of miR-323a-3p, while other processes were enriched for the other miRNA targets (Figure S15). Interestingly, migration-related terms were observed in the analysis of miR-449b-5p targets, which coincided with miR-449b-5p overexpression having the strongest decrease in HSVSMC migration among the seven miRNAs. For miR-892b, terms related to osteoblast differentiation, another vSMC phenotype linked to vascular disease,[23] were identified.

To understand how individual targets could contribute to the proliferative phenotype, we selected three targets for further characterization. We included *IGF2BP3*, as this gene is targeted by five miRNAs but also focused on other distinct targets with known roles in cell-cycle/SMC proliferation, such as *CCND1* (target of miR-449b-5p and miR-491-3p), which is a core cell-cycle gene, and *GJA1* (target of miR-323a-3p), associated with "SMC proliferation" GO terms. The decrease in *IGF2BP3*, *CCND1*, and *GJA1* mRNA levels upon miRNA overexpression was confirmed by RT-qPCR (except for miR-491-3p) (Figure 4D). To assess the contribution of the targets to HSVSMC proliferation, we performed small interfering RNA (siRNA)-mediated knockdown of the three targets individually (Figure S16). Only *CCND*1 knockdown showed a significant decrease in HSVSMC proliferation (Figure 4E). These data suggest that *IGF2BP3* does not mediate the effect on proliferation despite being a common target of five miRNAs. In contrast, *CCND1*, regulated by miR-449b-5p, might contribute to the proliferative phenotype.

Our target analysis revealed limited overlap of the candidate targets and a more unique candidate target signature for each miRNA. Some targets have relevance to cell-cycle regulation, and we showed that *CCND1*, target of miR-449b-5p, regulates HSVSMC proliferation.

Overexpression of individual miRNA candidates differentially regulates HSVSMCs and HSVECs

Because preservation of the function of the endothelium during vein grafting is key, we overexpressed the seven miRNAs in human saphenous vein ECs (HSVECs) and assessed the effect on proliferation based on EdU incorporation and flow cytometry (Figure 5A). No significant change in proliferation was observed for miR-323a-3p, miR-491-3p, miR-892b, miR-1827, and miR-5681b compared to miR-CTRL (Figure 5B). A significant decrease in proliferation was observed for miR-449b-5p and miR-4774-3p (Figure 5B). However, while a 98% and 95% decrease in proliferation was observed in HSVSMCs for miR-449b-5p and miR-4774-3p, respectively, the effect on EC was lower, with only a 61% decrease in proliferation for both miRNAs. We also assessed if the miRNA mimics had any toxic effect on HSVECs using a lactate dehydrogenase quantification. Similar to the result in HSVSMCs, no significant increase in cytotoxicity was reported in HSVECs (Figure 5C).

To understand the effect of overexpression of the seven miRNAs at a molecular level, we performed RNA-seq. In contrast to what was observed in HSVSMCs, the PCA did not reveal a clear separation between the miRNA overexpression condition and the miR-CTRL in HSVECs (Figure S17), suggesting no or a low effect of the miRNA overexpression on the transcriptome. Differential gene expression analysis identified changes for 3 to 61 genes across the different conditions, with no gene commonly regulated across the conditions (Figure 5D and Table S5), confirming a low effect on the transcriptome. As expected, some of the changes in ECs were previously identified in the HSVSMC RNA-seq (Figure 5D), showing some common but minimal gene regulation by the miRNAs across these two cell types.

We also visualized the expression of the 102 genes commonly downregulated across the overexpression of the miRNAs in HSVSMCs and involved in cell cycle within the HSVEC RNA-seq. We observed little difference between miRNA overexpression conditions and miR-CTRL for these genes in HSVECs (Figure 5E), in agreement with the lack of or low proliferation phenotype in this cell type. Equally, we visualized the expression of the miRNA candidate targets identified in the HSVSMC RNA-seq. Thirty-two of the 680 miRNA candidate targets had low or no expression in HSVECs, and the 648 expressed targets did not display a consistent downregulation across the three replicates in HSVEC samples (Figure S18). *CCND1*, a target of miR-449b-5p and miR-491-3p contributing to HSVSMC proliferation, does not show significant changes in HSVECs upon miRNA overexpression. Interestingly, we observed that the expression level of *CCND1* was lower in HSVECs (average 99 fragments per kilobase of transcript per million mapped reads [FPKM] in fetal bovine serum [FBS]/miR-CTRL) than in HSVSMCs (average 398 in IL-1α + PDGF-BB/miR-CTRL) (Figure S19), and this difference in expression could explain the different response to the miRNA overexpression.

As the endothelium could also be indirectly affected by the miRNA-mediated changes to the vSMCs via a paracrine effect, we exposed HSVECs to conditioned medium obtained from HSVSMCs treated with the mimics (Figure S20A) and assessed proliferation via EdU

Figure 5. Proliferation and transcriptomic changes upon overexpression of the seven candidate miRNAs in HSVECs

(A) Schematic of experimental design for assessing the effect of miRNA overexpression on HSVEC proliferation, cytotoxicity, and transcriptome. (B) Flow cytometric quantification of EdU incorporation in HSVECs transfected with the seven miRNA mimics versus miR-CTRL and lipofectamine-treated cells (mock) ($n = 3$). Statistical analyses were done using Iman-Conover non-parametric ranking followed by repeated-measures ANOVA. The p value was calculated for the comparison between miRNA-mimic treatment and miR-CTRL using Dunnett's test for multiple comparisons. On the graph, $^*p < 0.05$ and ns, non-significant. (C) Lactate dehydrogenase activity in HSVECs transfected with the seven miRNA mimics or miR-CTRL, as well as the mock transfection control ($n = 3$). Statistical analyses were done using Iman-Conover non-parametric ranking followed by repeated-measures ANOVA. (D) Number of significantly differentially expressed genes for each miRNA overexpression versus miR-CTRL based on RNA-seq in HSVECs. The number of genes commonly regulated by all miRNAs is indicated below. Hatched areas show the proportion of genes also regulated in HSVSMCs. (E) HSVEC expression profile (displayed as row Z score) of the cell-cycle genes commonly downregulated by all seven miRNAs in HSVSMCs. Ninety-six of the 102 genes were detected in HSVECs. Error bars on the graphs correspond to standard error of the mean. n corresponds to distinct biological replicates.

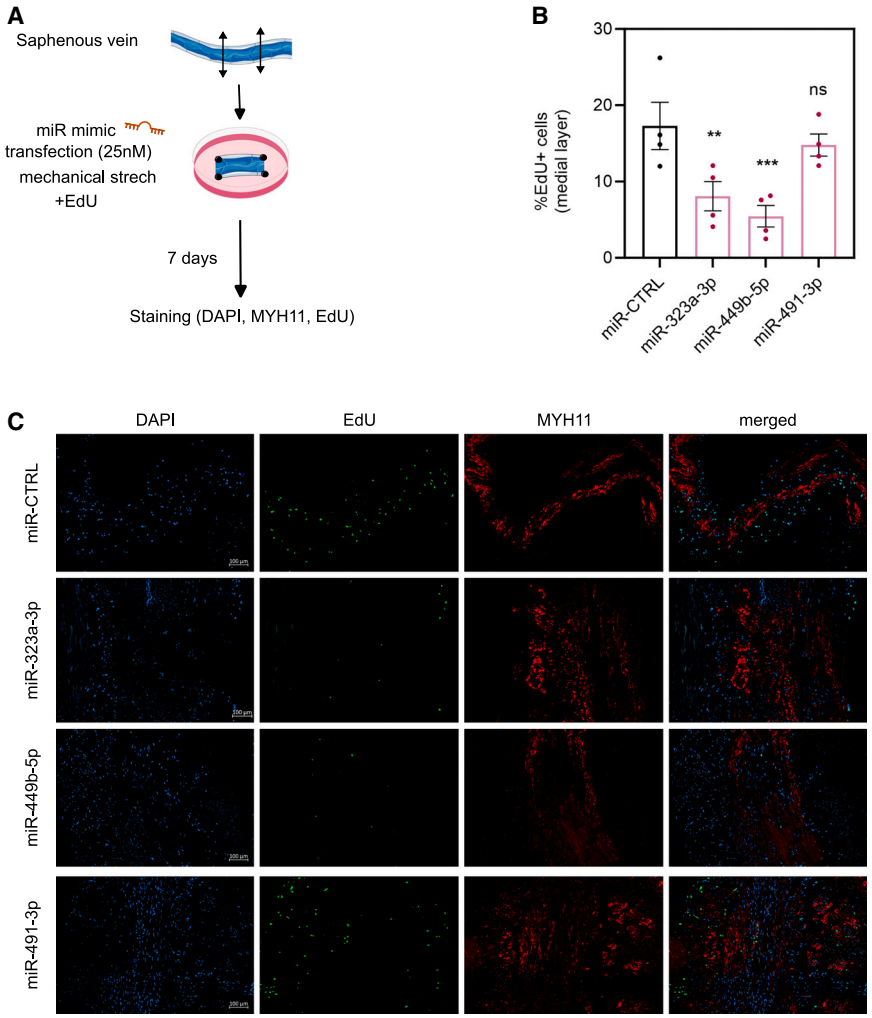

Figure 6. Reduced medial proliferation in human saphenous vein organ culture upon miR-323a-3p and miR-449b-5p overexpression

(A) Schematic of the miRNA-mimic treatment of the human saphenous vein. The remodeling is induced by mechanical stress followed by organ culture for 7 days. (B) Percentage of EdU-positive cells in the medial layer of human saphenous vein upon miRNA-mimic treatment after 7 days (n = 4). Statistical analyses were done using Iman-Conover non-parametric ranking followed by repeated-measures ANOVA. The p value was calculated for the comparison between miRNA-mimic treatment and miR-CTRL using Dunnett's test for multiple comparisons. On the graph, error bars correspond to standard error of the mean and $^{**}p < 0.01$, $^{***}p < 0.001$, and ns, non-significant. n correspond to distinct biological replicates. (C) Representative images of EdU, MYH11, and DAPI staining after miR-CTRL or miRNA-mimic treatment in the vein organ culture. Scale bars, 100 μm.

incorporation and flow cytometry. We observed that HSVECs cultured with conditioned medium from miR-CTRL-treated HSVSMCs showed a reduced proliferation compared to HSVECs cultured in EC medium (Figure S20B), showing that conditioned medium from HSVSMCs affects HSVEC proliferation. However, no significant difference was observed between the conditioned media from the seven miRNA mimics and miR-CTRL (Figure S20B), suggesting that, in this condition, the overexpression of the candidate miRNAs in HSVSMCs did not lead to a negative paracrine effect on HSVEC proliferation.

These data indicate that the miRNAs can strongly regulate HSVSMCs without significantly affecting the proliferation and transcriptome of HSVECs.

miR-323a-3p and miR-449b-5p overexpression decreased medial layer proliferation in a human *ex vivo* model of vein graft remodeling

To test the therapeutic potential of the seven candidate miRNAs, we aimed to assess their impact on proliferation in a diseased tissue setting. However, only miR-323a-3p and miR-491-3p showed complete sequence conservation in pig and mouse, precluding the use of these two important animal models of vein graft disease to test the seven miRNA candidates. Therefore, we decided to use an *ex vivo* human model of vein graft remodeling that has been previously used to test gene[24] and RNA-based therapy.[25,26]

We focused on miR-323a-3p, the only miRNA with targets showing an enrichment for "cell-cycle"-related GO terms, but also miR-449b-5p and miR-491-3p, as the knockdown of one of their targets (*CCND1*) was shown to affect HSVSMC proliferation *in vitro*. Mimic transfection was performed in vein sections while adding EdU to allow proliferation analysis, and the vein sections were cultured for 7 days (Figure 6A). We assessed if the mimic-mediated miRNA overexpression could still be detected at 7 days. Using RT-qPCR, we observed that the miRNA level was higher in the mimic-treated sample compared to miR-CTRL for all miRNAs in all three biological replicates, and we showed a significant change for miR-323a-3p (Figure S21). To quantify proliferation at 7 days, we performed staining for EdU. We also stained for the vSMC marker MYH11 to delineate the medial layer of the vein and quantify EdU-positive cells in this area. We observed a significant decrease in proliferating cells upon overexpression of miR-323a-3p and miR-449b-5p but not miR-491-3p (Figures 6B and 6C).

The decrease in medial proliferation in the *ex vivo* human vein culture model using miR-323a-3p and miR-449b-5p mimics highlighted the therapeutic potential of the overexpression of these two miRNAs.

DISCUSSION

Therapy targeting vSMC proliferation could prevent vascular remodeling across different diseases. Here, we considered the use of miRNA-based therapeutics and performed a high-throughput functional miRNA screen to unbiasedly identify miRNA mimics regulating vSMC proliferation. We focused our study on seven miRNAs with no previously reported role in vSMC proliferation and confirmed their effects on proliferation in different types of vSMCs. Their overexpression in HSVSMCs led to decreased proliferation, and migration for 5 of them, without any toxic effect, suggesting their potential in the context of vein graft failure. Transcriptomic analysis showed the regulation of a core network of cell-cycle genes for all seven miRNAs in agreement with the anti-proliferative phenotype. However, target analysis suggested distinct targets for each individual miRNA. Overexpression of the seven miRNAs shows no or little effect on proliferation, cytotoxicity, and gene expression changes in HSVECs, suggesting an HSVSMC-specific effect and an added potential for therapy. Using an *ex vivo* vein organ model, we showed that miR-323a-3p and miR-449b-5p overexpression reduced medial layer proliferation, highlighting their therapeutic potential.

Our study is based on a high-throughput screen using a library of 2,042 miRNAs corresponding to all miRNAs annotated in the miRBase at the time of the study design. Therefore, it constitutes a comprehensive resource of miRNA overexpression effects in vSMC proliferation, and we identified 417 and 715 miRNAs with a positive and negative effect on PASMC proliferation, respectively, providing a large number of candidates for further studies. As we aim to block vSMC proliferation, we focused on the anti-proliferative miRNAs, allowing the future development of an miRNA-based therapy using mimics or viral delivery for overexpression. For the selected seven miRNAs, we showed that the beneficial effect in HSVSMCs came from the exogenous miRNA expression, as we could not detect endogenous expression for the seven miRNA candidates. Therefore, the seven candidate miRNAs do not play a physiological role in HSVSMCs in the tested conditions but might regulate proliferation in other cell types and contexts when endogenously expressed. We also showed an anti-proliferative phenotype on vSMCs from different vascular beds, suggesting that the exogenous expression of the seven miRNAs could be beneficial in different disease contexts. The prospect of regulating the same miRNA in different diseases has been previously noted for several miRNAs involved in vSMC phenotypic changes.[14] For example, miR-21 ablation was shown to attenuate neointima formation in a mouse model of vein graft remodeling,[26] while miR-21 modulation also had an impact in the context of abdominal aortic aneurysm.[27] miR-34a was found among the top anti-proliferative miRNAs from the screen and was previously implicated in several cardiovascular diseases and considered as a promising therapeutic candidate.[28] However, miR-34a also regulates vascular senescence and inflammation processes[29] that might be detrimental in some specific disease contexts.

The transcriptomic analysis in HSVSMCs showed that overexpression of all seven miRNAs led to the downregulation of the same network of cell-cycle genes, in agreement with the shared anti-proliferative phenotype. To provide miRNA candidate targets with high confidence, we incorporated the list of downregulated genes in addition to a combination of several prediction tools. With this approach, we showed distinct target pools for each miRNA with no common target. *IGF2BP3* was identified as a candidate target for five miRNAs. However, despite *IGF2BP3*'s role in cell proliferation in cancer,[30] *IGF2BP3* knockdown did not affect HSVSMC proliferation. Our analysis revealed that six of the seven miRNAs have candidate targets involved in the cell cycle based on GO term annotation. Interestingly, our study of the cell-cycle gene *CCND1*, a target of miR-449b-5p and miR-491b-3p, confirmed its contribution to HSVSMC proliferation. In contrast, knockdown of *GJA1* did not show a decrease in HSVSMC proliferation, despite its vSMC proliferation GO terms annotation.

While the regulation of individual cell-cycle genes by each miRNA could be responsible for the anti-proliferative phenotype, each miRNA also targets different processes that could converge toward an anti-proliferative effect. Enrichment of "migration"-related terms was found for miR-449b-5p targets, and we know that pathological vSMCs display both a pro-migratory and a pro-proliferative phenotype with some connections between the two phenotypes.[31] For miR-892b, we found an enrichment of the term "negative regulation of osteoblast differentiation" for its targets. Recently, single-cell RNA-seq has revealed the diversity of differentiated vascular smooth phenotype in healthy and disease conditions with the identification of osteogenic-like SMCs.[23]

As we do not want a miRNA-based strategy to have a detrimental effect on the endothelium, we assessed the effect of miRNA overexpression on HSVECs and showed no significant or a limited effect on proliferation, gene expression changes, and cytotoxicity. Therefore, a therapeutic approach using mimics, and thus not relying on an SMC-specific delivery, could work for these miRNA candidates. Cell-type-specific effects of miRNAs have been previously reported[32] but are poorly understood. The different response is believed to be linked to different target availability due to a distinct transcriptome in each cell type. The miRNA candidate target identification was based on the HSVSMC RNA-seq, and our transcriptomic data in HSVECs showed that some of these targets have a different basal expression levels between those of vSMCs and ECs, with 32 targets not expressed in HSVECs. In particular, *CCND1*, a target of miR-449b-5p and miR-491-3p in HSVSMCs, showed a lower expression in HSVECs, and this difference of expression could explain its lack of regulation by the miRNAs in HSVECs. In addition, we considered the possibility of a detrimental effect of miRNA overexpression in HSVSMCs on HSVECs in a paracrine manner but showed no significant change in HSVEC proliferation using conditioned medium from mimic-transfected HSVSMCs. Altogether, our study showed that the seven miRNAs could be used to target vSMCs without affecting ECs.

Following our extensive *in vitro* analysis, we proceeded to test the miRNA candidates in a tissue setting. While there are animal models

of vein graft remodeling, such as mouse[26] and pig,[33] they have limitations, and their use for testing miRNAs will depend on the conservation of the miRNA in the studied species. Only two of the seven candidate miRNAs showed conservation across species. Ideally, we also wanted to test the miRNA mimics in the same tissue/setting in which the therapy will be delivered. Therefore, we tested the miRNA mimics in a human *ex vivo* vein graft model that uses an excess of saphenous vein obtained during bypass surgery. We showed that miR-323a-3p and miR-449b-5p, but not miR-491-3p, reduced medial layer proliferation, indicating therapeutic potential for these two miRNAs. Further work is needed to test all seven candidates in this model.

miRNA mimics have been used in therapy settings[18] and could be applied to veins *ex vivo* before grafting directly in the cardiac theater environment, thus minimizing the impact on current clinical practice. Importantly, our dose-response study *in vitro* showed an effect at a dose as low as 2 nM, suggesting the potential to use mimics at low concentration for therapy and the need for further optimization in the tissue setting. However, other overexpression and delivery methods, viral or non-viral,[17] might be necessary in vein graft settings to allow a targeted delivery to specific cell types or subtypes. Our study showed that each individual miRNA has potential for future therapy. However, as most of the miRNA targets are unique for each miRNA, a combination of several miRNAs might provide additional (or synergistic) beneficial effects to block vSMC proliferation. In addition, targeting the distinct vSMC phenotypes observed in the disease context[23] via miRNA-based therapy should also be considered. Future work will be required to test different combinations of miRNAs to target vSMC pathological phenotypes.

MATERIALS AND METHODS

Cell culture

HPASMCs, HCASMCs, and HUVSMCs were purchased from Lonza and cultured using the recommended media. HSVSMCs and HSVECs were isolated from medial explants. All donated tissues were obtained under proper informed consent, and the investigation conformed to the principles in the Declaration of Helsinki. HSVSMCs were obtained and maintained as previously described.[6] Briefly, HSVSMC culture was performed using SMC growth medium 2 (Promocell) supplemented with the SMC 2 medium supplement (Promocell), 10% FBS (Gibco), 2 mM L-glutamine (Invitrogen), 50 μg/mL penicillin (Invitrogen), and 50 μg/mL streptomycin (Invitrogen). HSVECs were obtained by enzymatic collagenase digestion of human saphenous veins (Ethics 15/ES/0094) as previously described.[34] Cells were maintained in EC growth medium (EGM-2 BulletKit, Lonza) supplemented with 2% FBS (Life Technologies) and penicillin-streptomycin (100 U/mL) (Gibco). All cells were used between passages 3 and 5 and kept at 37°C in a humidified atmosphere containing 5% CO_2.

High-content microscopy, high-throughput proliferation screening of miRNAs on HPASMCs

A library of 2,042 human miRNA mimics (Dharmacon, Thermo Fisher Scientific) was used to transfect HPASMCs at a concentration of 50 nM using RNAiMAX lipofectamine. Twelve hundred cells were plated per well in 384-well plates. Forty-eight hours post-transfection, the cells were pulsed with EdU for 24 h and fixed 72 h after transfection. Cells were stained with the Alexa Fluor 488 EdU Click-iT kit (Thermo Fisher Scientific) and counterstained with Hoechst 33342. High-content fluorescence images were acquired using the Image Xpress micro microscope (Molecular Devices) and analyzed using MetaXpress version 5.3.0.5 to assess total cell number and percentage of EdU-positive cells. miRNAs exerting a negative effect on cell number, i.e., likely toxic, were excluded from analysis by calculating a Z score of the total cell number per well and excluding those with a reduction in total cell count of ≥ 1.5 standard deviations compared to the median cell count value.

Four miR-CTRLs as well as siRNA targeting the ubiquitin C gene (siUBC) from Dharmacon were included in the screen.

The four miR-CTRLs were Dharmacon miRNA mimic negative controls #1, #2, #3, and #4.

siUBC consisted of the siGENOME smartpool from Dharmacon (seq #1, GUGAAGACCCUGACUGGUA; seq #2, AAGCAAAGA UCCAGGACAA; seq #3, GAAGAUGGACGCACCCUGU; and seq #4, GUAAGACCAUCACUCUCGA).

Screening validation experiments

The fluorescence-microscopy-based analysis of proliferation described above for the screen was used to validate the effects of the seven selected miRNA mimics (Dharmacon, Thermo Fisher Scientific) on HPASMCs (n = 4), HCASMCs (n = 3), and HUVSMCs (n = 3). Similar to the screen, this was done in a 384-well plate format using RNAimax lipofectamine and 50 nM miRNA mimics. To monitor proliferation rates, EdU was added to cells after 48 h and fixed after 72 h. Cells were stained, imaged, and analyzed as mentioned above. miR-CTRL-2 (miR-CTRL-2: cel-miR-239b miRIDIAN microRNA Mimic Negative Control Dharmacon #2, UUGUACUACACAAAAGUACUG) was used as a negative control.

miRNA-mimic-mediated transfection of HSVSMCs and HSVECs

Transient transfection of the seven miRNA mimics (Dharmacon, Thermo Fisher Scientific) or the miR-CTRL (miR-CTRL-1: cel-miR67 miRIDIAN microRNA Mimic Negative Control #1, UCACAACCUCCUAGAAAGAGUAGA) was performed with lipofectamine RNAiMAX (Life Technologies), following the manufacturer's guidelines, for 6 h in Opti-MEM (Life Technologies). A 50 nM miRNA mimic concentration was used in all experiments. For the dose-response experiments, we also included lower concentrations of mimics of 2 and 10 nM.

siRNA transfection of HSVSMCs

Transient transfection of 50 nM siRNA targeting either *GJA1* (Invitrogen, Thermo Fisher, siRNA ID 144485), *IGF2BP3* (Invitrogen, Thermo Fisher, siRNA ID 3066), *CCND1* (Invitrogen, Thermo Fisher siRNA ID 42828), or siControl (siCTRL, Invitrogen, Thermo Fisher

Silencer Negative Control No. 1 AM4611) was performed using lipofectamine RNAiMAX (Life Technologies), following the manufacturer's guidelines, for 6 h in Opti-MEM (Life Technologies). Five biological replicates were performed. Replicates with a level of knockdown less than 20% were excluded from downstream proliferation analysis.

RNA extraction, RT, and TaqMan qPCR analysis

Total RNA isolation was performed using QIAzol Lysis Reagent and the miRNEasy Mini Kit including the RNase-free DNase Set (Qiagen), according to the manufacturer's instructions. All RNA samples were stored at −80°C until required. miRNA RT to cDNA utilized the Applied Biosystems miRNA Reverse Transcription Kit. cDNA was synthesized from total RNA (2 ng/μL RNA per reaction) using the MultiScribe Reverse Transcriptase kit (Life Technologies) and miRNA-specific RT probes or random primers. Thermal cycling conditions for synthesis involved 30-min incubations at 16°C and 42°C followed by a 5-min denaturation at 85°C. The reaction concluded with an indefinite hold at 4°C. After synthesis, all samples were stored at −20°C until required. Target-dependent, quantitative real-time PCR was later performed using TaqMan (Thermo Fisher Scientific) gene expression assays. TaqMan quantitative real-time PCR was performed using available TaqMan Gene Expression probes (Table S6) following the manufacturer's protocol (Thermo Fisher Scientific). RNU48 was used as a housekeeping gene for the normalization of RT-qPCR analysis of miRNAs. UBC was used as a housekeeping gene for the normalization of RT-qPCR analysis of protein-coding genes. Undetermined Ct values were replaced by 40, the number of qPCR cycles for a typical qPCR run. Quantification of gene expression was analyzed as a relative change of gene expression using the 2(−Delta Delta Ct) method as previously described.[35]

Details of TaqMan probes used for RT-qPCR analysis can be found in Table S6.

Assessment of proliferation using EdU incorporation followed by flow cytometry

Proliferation was assessed using a DNA EdU incorporation assay on a six-well plate format. HSVSMCs were sent into quiescence in 0.2% FBS medium for 48 h prior to transfection. Six hours after mimic or siRNA transfection, the cells were treated with 10 ng/mL IL-1α and 20 ng/mL PDGF-BB for 48 h in the presence of EdU. HSVECs were sent into quiescence in 0.2% FBS medium for 12 h prior to transfection. Six hours after miRNA-mimic or miR-CTRL transfection, cells were cultured in 10% FBS for 48 h in the presence of EdU. Single-cell suspensions of HSVSMCs and HSVECs were fixed for a minimum of 1 h in 70% ethanol. EdU incorporation was quantified using the Click-iT EdU Proliferation assay with an Alexa Fluor 488 antibody according to the manufacturer's protocol (Life Technologies). Cells were resuspended in PBS and analyzed by flow cytometry on the BD LSR5 Fortessa Analytic Flow Cytometer using a minimum of 10,000 events. Gating was performed using FlowJo software. One replicate of HSVSMCs transfected with miR-4774-3p was excluded from our analysis as the minimum number of events in flow cytometry was not obtained.

Assessment of proliferation using MKI67 staining

HSVSMCs were cultured, sent into quiescence in 0.2% FBS medium, transfected with miRNA mimics at a final dose of 50 nM, and treated with IL-1α and PDGF-BB as previously described, on sterile glass coverslips. Forty-eight hours after induction of proliferation, the medium was removed and the cells were washed 2× in sterile Dulbecco's phosphate-buffered saline (PBS) (Gibco 14190-094). The cells were fixed in 2% paraformaldehyde for 30 min at room temperature and permeabilized using 0.1% Triton X-100 (Dow) for 20 min at room temperature. Cells were blocked for 1 h in fish serum blocking buffer (Thermo Fisher Scientific) at room temperature and then stained overnight at 4°C with rabbit anti-human Ki-67 monoclonal antibody (SP6) (Invitrogen MA5-14520) at 1:500. After primary antibody incubation, the cells were washed 1× with PBS and incubated with goat anti-rabbit Alexa Fluor 488 at 1:500 dilution (Thermo Fisher Scientific) for 1 h at room temperature, protected from light. The cells were washed 2× in PBS and mounted using Prolong Gold Antifade Mountant with DAPI (Invitrogen P36935, Thermo Fisher Scientific). The cells were imaged on a Zeiss Axioscan 7 slide scanner (Carl Zeiss AG) with fixed exposure times between conditions. Images were analyzed using QuPath 0.4.3 open-source software.[36] A new project was created for each biological replicate, images were imported, and file names were scrambled using the "mask image names" function. A single image was opened, and the AF488 (KI67) channel was switched off. Approximately 200 DAPI-positive cells were counted using the "cell counter" function, before the AF488 (KI67) channel switched back on and the DAPI channel switched off. The number of KI-67-positive cells was counted among the 200 DAPI-positive population and the percentage of KI-67-positive cells calculated. This process was repeated for each image in a given project, with file names unscrambled.

Wound healing assay

HSVSMCs were plated in six-well plates and sent into quiescence in 0.2% FBS medium for 48 h prior to wound induction and stimulation. The cells were next transfected with 50 nM miRNA-mimic or miR-CTRL for 6 h before being scratched with a sterile 1-mL pipette tip. Subsequently, scratched HSVSMCs were stimulated with 10 ng/mL IL-1α and 20 ng/mL PDGF-BB for 48 h. Post-stimulation, bright-field microscopy images were taken for quantification of wound area closure using ImageJ.

Lactate dehydrogenase cytotoxicity assay

Changes in cytotoxicity following miRNA overexpression were determined using the Lactate Dehydrogenase (LDH)-Glow Cytotoxicity Assay kit (#J2380, Promocell), following the manufacturer's guidelines. To determine maximum LDH release, vehicle-only cells were treated with 20 μL of 10% Triton X-100 per 100 μL for 15 min. Cell culture medium, which was not conditioned by cells, was used to determine background luminescence. Supernatants were collected and stored at −20°C in LDH Storage Buffer prepared according to the

manufacturer's instructions. Samples were combined with LDH Detection Reagent, prepared following the manufacturer's instructions, and luminescence was recorded after a 60-min incubation at room temperature using a VANTAstar microplate reader (BMG Labtech).

Senescence-associated β-galactosidase assay in HSVSMCs

Senescence-associated β-galactosidase in HSVSMC lysates was quantified using the Senescence β-Galactosidase Activity Assay Kit (Fluorescence, Plate-Based) (Cell Signaling Technology). Measurement was done on cell lysates with the same total protein concentration. Absorbance at 405 nm was measured using a Molecular Devices microplate reader. Cells treated with bleomycin (1 μg/mL) were used as a positive control for senescence induction.

Mimic treatment of the *ex vivo* human saphenous vein organ model

Human saphenous vein culture was performed as previously described.[25] Briefly, 5- to 10-mm segments of excess human saphenous vein were transfected with miRNA mimics at a final concentration of 25 nM using lipofectamine RNAiMax (Thermo Fisher Scientific) for at least 6 h. Then the segments were cut open, pinned down, and cultured in DMEM supplemented with 100 mg/mL penicillin, 100 IU/mL streptomycin, 2 mM L-glutamine, and 10% (v/v) FBS, and EdU was added at a concentration of 10 μM. Medium was changed every 2–3 days. Four biological replicates were performed.

After 7 days, vein segments were immersed in 4% paraformaldehyde (PFA) overnight and then transferred to 70% ethanol until paraffin embedding. Five-micrometer-thick sections were collected and then processed with immunostaining. Paraffin-wax-embedded sections were assessed using the Click-iT EdU Cell Proliferation Kit (Thermo Fisher Scientific). Paraffin-wax-embedded sections were deparaffinized in xylene (2 × 5-min washes) and 2 × 100% ethanol washes (1 min per wash), followed by serial washes using 90%, 80%, and 70% ethanol (1 min each), ending in ultrapure water and followed by a PBS wash. The tissue was then permeabilized with 0.5% Triton X-100/PBS for 45 min. After serial 3% BSA/PBS washes, the tissue was incubated with a Click-iT EdU reaction cocktail for 30 min in the dark at room temperature. The tissue was then washed with serial 3% BSA/PBS washes, and fish serum (37527, Thermo Fisher Scientific) was used as blocking solution for 1 h at room temperature in the dark. Primary rabbit anti-human antibody for MYH11 (Abcam, ab224804, 1:100 dilution) was diluted in the blocking solution and applied to the tissue overnight at 4°C. The next day, the tissue was washed 3 × 5 min using PBS containing 0.1%Triton X-100. Secondary antibody was prepared in blocking solution (goat anti-rabbit IgG AF647, A21245, Life Technologies, Thermo Fisher Scientific, 1:500 dilution) and added on sections for 2 h protected from light and at room temperature. Following three washes with PBS, the tissue was mounted using ProLong Gold Antifade Mountant containing DAPI.

Image quantification was performed using Qupath. MYH11 staining was used to highlight the medial vascular area of the vein, and four or five regions of interest overlapping this area across the full length of the vein tissue were selected for EdU and DAPI quantification (regions were encircled using the Measure function of Qupath). For each region, the percentage of EdU-positive cells over the total number of nuclei (DAPI) were calculated. The average of the percentage of EdU-positive cells across the four or five selected areas was calculated.

Statistical analysis of *in vitro* results

Biological replicates for HPASMCs, HCASMCs, and HUVSMCs correspond to experiments performed on cells derived from different vials. Biological replicates for primary cells HSVSMCs and HSVECs correspond to experiments performed using distinct patient-derived cell lines. Data are expressed as bar charts of mean ± standard error of the mean (SEM) with individual datapoints superimposed to show full data distribution. Statistical tests used to assess statistical significance are indicated in each figure legend. GraphPad Prism version 10 was used for statistical analysis. For RT-qPCR, statistical analysis was performed on delta Ct, under the assumption of log normality as previously described,[37] using a repeated-measures ANOVA. For EdU incorporation data determined by flow cytometry in HSVSMCs, we know that the data follow a normal distribution based on a Shapiro-Wilk test on internal data (data not shown). For the other experimental data, as the sample size was <5, normal distribution could not be assessed accurately. Therefore, data were subjected to Iman-Conover non-parametric ranking followed by repeated-measures one-way ANOVA. When the numbers of replicates were different across conditions, the statistical analysis was done using a mixed-effects model. Multiple comparisons were performed using Dunnett's test when comparing to one control group or using Tukey's test when comparing all groups.

Analysis of bulk RNA-seq following miRNA overexpression

RNA-seq was performed on RNA-extracted and DNase-treated samples using the miRNeasy mini kit (Qiagen) obtained from three replicates of miRNA overexpression, including controls, HSVSMCs, and HSVECs. Library preparation was prepared after poly(A) mRNA selection using the NEBNext Ultra II Directional RNA Library Prep Kit for Illumina following the manufacturer's instructions (NEB). Sequencing was performed on an Illumina NovSeq600 using a 2 × 150 paired-end configuration. Gene quantification (read count and FPKM) was obtained using RSEM (options: -bowtie2 -pairedend), based on human GRCh38 genome annotation and GENCODE transcriptome annotation (release 25). Raw and processed data of the RNA-seq performed in HSVSMCs and HSVECs are available at the GEO database under accession series GEO: GSE253004 with subseries GEO: GSE253003 for HSVSMC data and GEO: GSE253002 for the HSVEC data. Downstream analysis was done in RStudio version 2023.09.0 with R version 4.3.1. PCA and differential expression were performed utilizing DEseq2 version 1.42.0.[38] Removal of batch/patient effect was performed using the limma version 3.58.1 removeBatchEffect function. Differential expression analysis using DESeq2 was done using the Wald test followed by the Benjamini and Hochberg method for multiple correction. Significantly differentially expressed genes were identified using

the following thresholds: absolute fold change ≥ 2, adjusted p value 0.01, and a minimum expression of 2 FPKM in at least two of the miR-CTRL/miR-mimic samples. Gene set enrichment analysis was performed using clusterProfiler version 4.10.0[39] for each set of comparisons (miRNA mimics versus miR-CTRL) focusing on the GO term biological process with Org.Hs.eg.db_3.18.0. Adjusted p values were obtained after Benjamini and Hochberg correction. GO enrichment analysis of the 125 common downregulated genes and the miRNA candidate targets was performed using TopGo version 2.54.0 with Org.Hs.eg.db_3.18.0. Visualization of genes involved in the KEGG cell-cycle pathway hsa04110 was obtained using Pathview version 1.42.0.[40] The heatmap of gene expression (displayed as the Z score of log2(FPKM + 1)) based on RNA-seq was obtained using pheatmap package version 1.0.12.

multimiR target prediction and filtering

miRNA target prediction was performed using the multimiR R package.[22] Differentially expressed genes following overexpression of each miRNA were considered targets if they were found among the top 50% of targets (based on prediction score) in two miRNA prediction tools.

Illustrations

Most illustrations were obtained from Bioicons (https://bioicons.com/) as indicated below. Smooth-muscle-fiber, multiwell-plate-3d, vein, and arrow-up-long icons by Servier https://smart.servier.com/ are licensed under CC-BY 3.0. CC_dish icon by Marcel Tisch https://twitter.com/MarcelTisch is licensed under CC0. Fluoresent_bead_yellow and Fluoresent_bead_orange icons by B-Gideon-Bergheim are licensed under CC0. Endothelium illustration was obtained from https://smart.servier.com/.

Other methods

Methods related to supplemental figures are included in the supplemental information.

DATA AND CODE AVAILABILITY

Raw and processed data from the RNA-seq have been deposited in the GEO database (GEO: GSE253004 with subseries GEO: GSE253003 for HSVSMC data and GEO: GSE253002 for the HSVEC data). Other data can be obtained upon request.

ACKNOWLEDGMENTS

We would like to thank Jean Iyinikkel for conducting experiments in human saphenous vein cell lines and her contribution to the analysis of these experiments and the RNA-seq. Flow cytometry data were generated with support from the QMRI Flow Cytometry and Cell Sorting Facility, University of Edinburgh. Bioinformatics analysis has made use of the resources provided by the Edinburgh Compute and Data Facility (http://www.ecdf.ed.ac.uk/).

J.R., A.B., and A.H.B. are supported by the BHF Chair of Translational Cardiovascular Sciences (CH/11/2/28733). S.Z. is supported by grant AIRC IG2020 Id24529. S.Z. and M.G. are supported by a grant from the National Center for Gene Therapy and Drugs based on RNA Technology in the frame of the National Recovery and Resilience Plan (PNRR) financed by the European Union – NextGeneration EU CUP J93C22000530006. A.H.B. is also supported by a BHF program grant (RG/20/5/34796) as well as the ERC Advanced Grant Vascmir (338991).

AUTHOR CONTRIBUTIONS

A.H.B., M.G., and S.Z. proposed the hypothesis and supervised the study. L.B. and N.A.R.R. performed the screen, and N.A.R.R. performed the validation experiments. The experiments in human saphenous vein cell lines were conducted by S.D.B., M.D.B., D.K., A.N.D.C., and V.M., and the analyses of the experiments were performed by J.R., E.K., S.D.B., D.K., and A.N.D.C. G.K. performed the experiments in the *ex vivo* saphenous vein model. RNA-seq analyses were conducted by J.R. and E.K. with the help of D.K. J.R. wrote the manuscript with the help of E.K. M.D.B., F.V., K.M., M.B., and A.B. contributed to the discussion. All authors reviewed the manuscript.

DECLARATION OF INTERESTS

The authors declare the following financial interests/personal relationships that may be considered potential competing interests: A.H.B., M.G., and S.Z. are named inventors on a patent application related to this work (PCT/GB2023/052170).

SUPPLEMENTAL INFORMATION

Supplemental information can be found online at https://doi.org/10.1016/j.ymthe.2024.12.037.

REFERENCES

1. Lyle, A.N., and Taylor, W.R. (2019). The pathophysiological basis of vascular disease. Lab. Invest. *99*, 284–289. https://doi.org/10.1038/s41374-019-0192-2.

2. Gaudino, M., Antoniades, C., Benedetto, U., Deb, S., Di Franco, A., Di Giammarco, G., Fremes, S., Glineur, D., Grau, J., He, G.-W., et al. (2017). Mechanisms, Consequences, and Prevention of Coronary Graft Failure. Circulation *136*, 1749–1764. https://doi.org/10.1161/circulationaha.117.027597.

3. Bacakova, L., Travnickova, M., Filova, E., Matějka, R., Stepanovska, J., Musilkova, J., Zarubova, J., and Molitor, M. (2018). The role of vascular smooth muscle cells in the physiology and pathophysiology of blood vessels. In Muscle Cell and Tissue, K. Sakuma, ed. (InTech), pp. 229–257. https://doi.org/10.5772/intechopen.77115.

4. Bochaton-Piallat, M.L., and Bäck, M. (2018). Novel concepts for the role of smooth muscle cells in vascular disease: towards a new smooth muscle cell classification. Cardiovasc. Res. *114*, 477–480. https://doi.org/10.1093/cvr/cvy031.

5. Wang, D., Uhrin, P., Mocan, A., Waltenberger, B., Breuss, J.M., Tewari, D., Mihaly-Bison, J., Huminiecki, Ł., Starzyński, R.R., Tzvetkov, N.T., et al. (2018). Vascular smooth muscle cell proliferation as a therapeutic target. Part 1: molecular targets and pathways. Biotechnol. Adv. *36*, 1586–1607. https://doi.org/10.1016/j.biotechadv.2018.04.006.

6. Ballantyne, M.D., Pinel, K., Dakin, R., Vesey, A.T., Diver, L., Mackenzie, R., Garcia, R., Welsh, P., Sattar, N., Hamilton, G., et al. (2016). Smooth Muscle Enriched Long Noncoding RNA (SMILR) Regulates Cell Proliferation. Circulation *133*, 2050–2065. https://doi.org/10.1161/CIRCULATIONAHA.115.021019.

7. Daemen, J., and Serruys, P.W. (2007). Drug-eluting stent update 2007: part I. A survey of current and future generation drug-eluting stents: meaningful advances or more of the same? Circulation *116*, 316–328. https://doi.org/10.1161/CIRCULATIONAHA.106.621342.

8. Roopmani, P., Sethuraman, S., Satheesh, S., and Maheswari Krishnan, U. (2016). The metamorphosis of vascular stents: passive structures to smart devices. RSC Adv. *6*, 2835–2853. https://doi.org/10.1039/c5ra19109b.

9. Baker, A.H., Mehta, D., George, S.J., and Angelini, G.D. (1997). Prevention of vein graft failure: potential applications for gene therapy. Cardiovasc. Res. *35*, 442–450. https://doi.org/10.1016/s0008-6363(97)00116-8.

10. Southerland, K.W., Frazier, S.B., Bowles, D.E., Milano, C.A., and Kontos, C.D. (2013). Gene therapy for the prevention of vein graft disease. Transl. Res. *161*, 321–338. https://doi.org/10.1016/j.trsl.2012.12.003.

11. Bartel, D.P. (2004). MicroRNAs: genomics, biogenesis, mechanism, and function. Cell *116*, 281–297. https://doi.org/10.1016/s0092-8674(04)00045-5.

12. Vishnoi, A., and Rani, S. (2017). MiRNA Biogenesis and Regulation of Diseases: An Overview. Methods Mol. Biol. *1509*, 1–10. https://doi.org/10.1007/978-1-4939-6524-3_1.

13. Wojciechowska, A., Osiak, A., and Kozar-Kamińska, K. (2017). MicroRNA in cardiovascular biology and disease. Adv. Clin. Exp. Med. *26*, 868–874. https://doi.org/10.17219/acem/62915.

14. Vacante, F., Denby, L., Sluimer, J.C., and Baker, A.H. (2019). The function of miR-143, miR-145 and the MiR-143 host gene in cardiovascular development and disease. Vascul. Pharmacol. *112*, 24–30. https://doi.org/10.1016/j.vph.2018.11.006.

15. Wang, G., Luo, Y., Gao, X., Liang, Y., Yang, F., Wu, J., Fang, D., and Luo, M. (2023). MicroRNA regulation of phenotypic transformations in vascular smooth muscle: relevance to vascular remodeling. Cell. Mol. Life Sci. *80*, 144. https://doi.org/10.1007/s00018-023-04793-w.

16. Wang, D., and Atanasov, A.G. (2019). The microRNAs Regulating Vascular Smooth Muscle Cell Proliferation: A Minireview. Int. J. Mol. Sci. *20*, 324. https://doi.org/10.3390/ijms20020324.

17. Bayraktar, E., Bayraktar, R., Oztatlici, H., Lopez-Berestein, G., Amero, P., and Rodriguez-Aguayo, C. (2023). Targeting miRNAs and Other Non-Coding RNAs as a Therapeutic Approach: An Update. Noncoding. RNA *9*, 27. https://doi.org/10.3390/ncrna9020027.

18. Iacomino, G. (2023). miRNAs: The Road from Bench to Bedside. Genes *14*, 314. https://doi.org/10.3390/genes14020314.

19. Rodrigues Lopes, I., Silva, R.J., Caramelo, I., Eulalio, A., and Mano, M. (2019). Shedding light on microRNA function via microscopy-based screening. Methods *152*, 55–64. https://doi.org/10.1016/j.ymeth.2018.09.011.

20. Eulalio, A., Mano, M., Dal Ferro, M., Zentilin, L., Sinagra, G., Zacchigna, S., and Giacca, M. (2012). Functional screening identifies miRNAs inducing cardiac regeneration. Nature *492*, 376–381. https://doi.org/10.1038/nature11739.

21. Gabisonia, K., Prosdocimo, G., Aquaro, G.D., Carlucci, L., Zentilin, L., Secco, I., Ali, H., Braga, L., Gorgodze, N., Bernini, F., et al. (2019). MicroRNA therapy stimulates uncontrolled cardiac repair after myocardial infarction in pigs. Nature *569*, 418–422. https://doi.org/10.1038/s41586-019-1191-6.

22. Ru, Y., Kechris, K.J., Tabakoff, B., Hoffman, P., Radcliffe, R.A., Bowler, R., Mahaffey, S., Rossi, S., Calin, G.A., Bemis, L., and Theodorescu, D. (2014). The multiMiR R package and database: integration of microRNA–target interactions along with their disease and drug associations. Nucleic Acids Res. *42*, e133. https://doi.org/10.1093/nar/gku631.

23. Yap, C., Mieremet, A., De Vries, C.J.M., Micha, D., and De Waard, V. (2021). Six Shades of Vascular Smooth Muscle Cells Illuminated by KLF4 (Krüppel-Like Factor 4). Arterioscler. Thromb. Vasc. Biol. *41*, 2693–2707. https://doi.org/10.1161/atvbaha.121.316600.

24. George, S.J., Lloyd, C.T., Angelini, G.D., Newby, A.C., and Baker, A.H. (2000). Inhibition of late vein graft neointima formation in human and porcine models by adenovirus-mediated overexpression of tissue inhibitor of metalloproteinase-3. Circulation *101*, 296–304. https://doi.org/10.1161/01.cir.101.3.296.

25. Mahmoud, A.D., Ballantyne, M.D., Miscianinov, V., Pinel, K., Hung, J., Scanlon, J.P., Iyinikkel, J., Kaczynski, J., Tavares, A.S., Bradshaw, A.C., et al. (2019). The Human-Specific and Smooth Muscle Cell-Enriched LncRNA SMILR Promotes Proliferation by Regulating Mitotic CENPF mRNA and Drives Cell-Cycle Progression Which Can Be Targeted to Limit Vascular Remodeling. Circ. Res. *125*, 535–551. https://doi.org/10.1161/circresaha.119.314876.

26. McDonald, R.A., White, K.M., Wu, J., Cooley, B.C., Robertson, K.E., Halliday, C.A., McClure, J.D., Francis, S., Lu, R., Kennedy, S., et al. (2013). miRNA-21 is dysregulated in response to vein grafting in multiple models and genetic ablation in mice attenuates neointima formation. Eur. Heart J. *34*, 1636–1643. https://doi.org/10.1093/eurheartj/eht105.

27. Maegdefessel, L., Azuma, J., Toh, R., Deng, A., Merk, D.R., Raiesdana, A., Leeper, N.J., Raaz, U., Schoelmerich, A.M., McConnell, M.V., et al. (2012). MicroRNA-21 Blocks Abdominal Aortic Aneurysm Development and Nicotine-Augmented Expansion. Sci. Transl. Med. *4*, 122ra22. https://doi.org/10.1126/scitranslmed.3003441.

28. Hua, C.C., Liu, X.M., Liang, L.R., Wang, L.F., and Zhong, J.C. (2021). Targeting the microRNA-34a as a Novel Therapeutic Strategy for Cardiovascular Diseases. Front. Cardiovasc. Med. *8*, 784044. https://doi.org/10.3389/fcvm.2021.784044.

29. Raucci, A., Macrì, F., Castiglione, S., Badi, I., Vinci, M.C., and Zuccolo, E. (2021). MicroRNA-34a: the bad guy in age-related vascular diseases. Cell. Mol. Life Sci. *78*, 7355–7378. https://doi.org/10.1007/s00018-021-03979-4.

30. Bell, J.L., Wächter, K., Mühleck, B., Pazaitis, N., Köhn, M., Lederer, M., and Hüttelmaier, S. (2013). Insulin-like growth factor 2 mRNA-binding proteins (IGF2BPs): post-transcriptional drivers of cancer progression? Cell. Mol. Life Sci. *70*, 2657–2675. https://doi.org/10.1007/s00018-012-1186-z.

31. Gerthoffer, W.T. (2007). Mechanisms of Vascular Smooth Muscle Cell Migration. Circ. Res. *100*, 607–621. https://doi.org/10.1161/01.res.0000258492.96097.47.

32. Rogg, E.-M., Abplanalp, W.T., Bischof, C., John, D., Schulz, M.H., Krishnan, J., Fischer, A., Poluzzi, C., Schaefer, L., Bonauer, A., et al. (2018). Analysis of Cell Type-Specific Effects of MicroRNA-92a Provides Novel Insights Into Target Regulation and Mechanism of Action. Circulation *138*, 2545–2558. https://doi.org/10.1161/circulationaha.118.034598.

33. Schachner, T., Laufer, G., and Bonatti, J. (2006). In vivo (animal) models of vein graft disease. Eur. J. Cardiothorac. Surg. *30*, 451–463. https://doi.org/10.1016/j.ejcts.2006.06.015.

34. Girao-Silva, T., Fonseca-Alaniz, M.H., Oliveira Dallan, L.A., Valadao, I.C., Oliveira da Rocha, G.H., Krieger, J.E., and Miyakawa, A.A. (2023). Human saphenous vein endothelial cell isolation and exposure to controlled levels of shear stress and stretch. J. Vis. Exp. *194*, e65122. https://doi.org/10.3791/65122.

35. Livak, K.J., and Schmittgen, T.D. (2001). Analysis of relative gene expression data using real-time quantitative PCR and the 2(-Delta Delta C(T)) Method. Methods *25*, 402–408. https://doi.org/10.1006/meth.2001.1262.

36. Bankhead, P., Loughrey, M.B., Fernández, J.A., Dombrowski, Y., McArt, D.G., Dunne, P.D., McQuaid, S., Gray, R.T., Murray, L.J., Coleman, H.G., et al. (2017). QuPath: Open source software for digital pathology image analysis. Sci. Rep. *7*, 16878. https://doi.org/10.1038/s41598-017-17204-5.

37. Ganger, M.T., Dietz, G.D., and Ewing, S.J. (2017). A common base method for analysis of qPCR data and the application of simple blocking in qPCR experiments. BMC Bioinformatics *18*, 534. https://doi.org/10.1186/s12859-017-1949-5.

38. Love, M.I., Huber, W., and Anders, S. (2014). Moderated estimation of fold change and dispersion for RNA-seq data with DESeq2. Genome Biol. *15*, 550. https://doi.org/10.1186/s13059-014-0550-8.

39. Wu, T., Hu, E., Xu, S., Chen, M., Guo, P., Dai, Z., Feng, T., Zhou, L., Tang, W., Zhan, L., et al. (2021). clusterProfiler 4.0: A universal enrichment tool for interpreting omics data. Innovation. *2*, 100141. https://doi.org/10.1016/j.xinn.2021.100141.

40. Luo, W., and Brouwer, C. (2013). Pathview: an R/Bioconductor package for pathway-based data integration and visualization. Bioinformatics *29*, 1830–1831. https://doi.org/10.1093/bioinformatics/btt285.

YMTHE, Volume *33*

Supplemental Information

Functional screening identifies miRNAs with a novel function inhibiting vascular smooth muscle cell proliferation

Julie Rodor, Eftychia Klimi, Simon D. Brown, Georgios Krilis, Luca Braga, Nadja A.R. Ring, Margaret D. Ballantyne, Despoina Kesidou, Aurelie Nguyen Dinh Cat, Vladislav Miscianinov, Francesca Vacante, Katarina Miteva, Matthew Bennett, Abdelaziz Beqqali, Mauro Giacca, Serena Zacchigna, and Andrew H. Baker

Supplemental methods

Caspase-3 assay for apoptosis analysis in HSVSMCs

Caspase-3 activity in HSVSMC lysates was quantified colorimetrically using the Caspase-3 Assay Kit from Abcam (ab39401), according to the manufacturer's protocol. Measurement was done on cell lysates with the same total protein concentration. Absorbance at 405 nm was measured using a Molecular Devices microplate reader. Cells treated with MG-115 at 1 μM concentration were used as a positive control.

SMC-condition medium stimulation of HSVECs

Human saphenous vein smooth muscle cells conditioned media (CM-SMC) from each non transfected and transfected experimental conditions including transfection with each 7 miRNA mimics were collected, centrifuged at 1000 g for 10 min at 4°C and sterile-filtered with 0.2 μm filters (Millipore). In 6 well-plates, 12 hours-quiescent HSVECs were stimulated with 500 mL of CM-SMC were added to 500 mL of EC basal medium with 10 μM EdU for 48 hours.

Proliferation was assessed using the Click-it EdU (5-Ethynyl-2′-deoxyuridine) 488 Proliferation assay (Life Technologies, UK) as per manufacturer's instructions. Cells were then dissociated and fixed in ice cold 70 % ethanol for EdU flow cytometry analysis. EdU incorporation was confirmed using anti-EdU 488 antibody.

Network analysis and visualisation

Genes commonly regulated by all miRNAs and candidate targets of each miRNA were considered. Genes involved in cell cycle regulation were extracted based on the GO Term annotation GO:0007049. Network analysis was done on these 176 genes. Gene interactions were obtained using STRING version 12.0 (https://string-db.org/) with default parameters. Visualisation of the network was performed using Cytoscape version 3.9.1. Genes commonly regulated by all miRNAs were placed at the centre of the network while targets were placed at the periphery.

Supplemental Tables

Table S1: miRNA screen result in HPASMC (Excel file).

Table S2: Differentially expressed genes between each miRNA mimic condition versus miR-CTRL in HSVSMC (Excel file).

Table S3: Gene set enrichment analysis (Biological Process GO Terms) for the differentially expressed genes between each miRNA mimic condition versus miR-CTRL in HSVSMC (Excel file).

Table S4: Candidate target genes for each candidate miRNA based on their downregulation in the HSVSMC RNAseq and their prediction by at least two prediction tools (Excel file).

Table S5: Differentially expressed genes between each miRNA mimic condition versus miR-CTRL in HSVEC (Excel file).

Table S6: TaqMan probes used for qRT-PCR analysis

Species	miRNA ID	TaqMan Assay ID
Human	hsa-miR-323-3p	002227
Human	hsa-miR-1827	002814
Human	hsa-miR-5681b	476577_mat
Human	hsa-miR-4774-3p	462836_mat
Human	hsa-miR-491-3p	002360
Human	hsa-miR-449b	001608
Human	hsa-miR-892b	002214
Human	RNU48	001006
Human	MKI67	Hs04260396_g1
Human	CCND1	Hs00765553_m1
Human	GJA1	Hs00748445_s1
Human	IGF2BP3	Hs00559907_g1
Human	UBC	Hs01871556_s1

Supplemental Figures

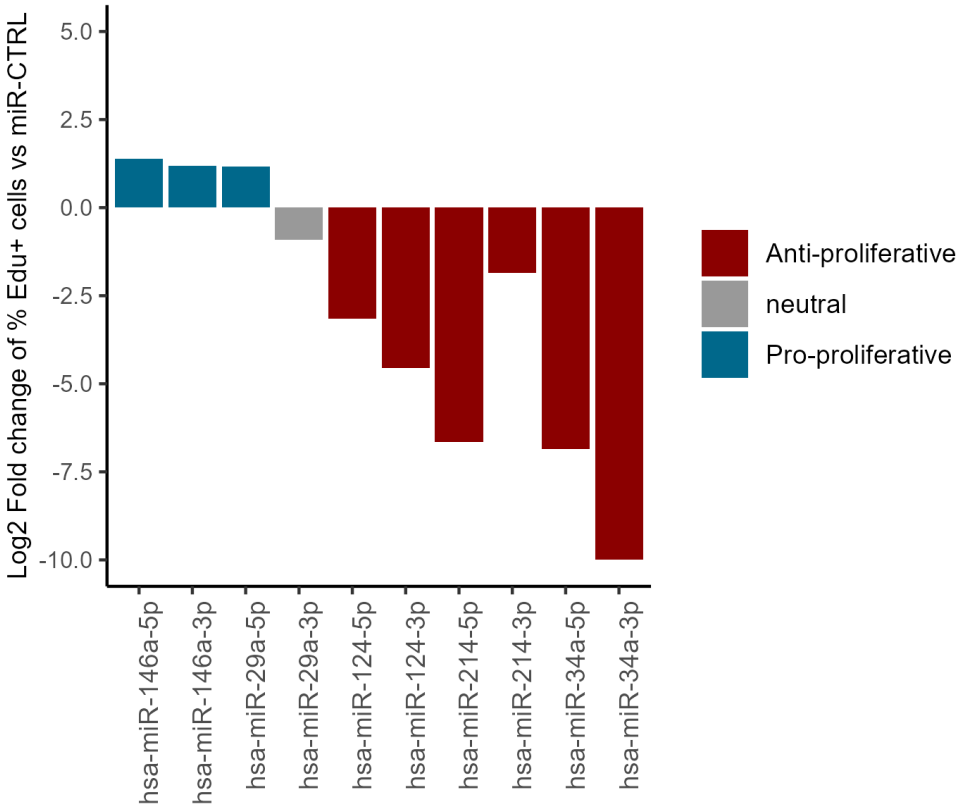

Figure S1. miRNAs with known effect on SMC proliferation (pro-proliferative: miR-146a and miR-29a, and anti-proliferative: miR-124, miR-214 and miR-34a) showed expected changes in the high-throughput high content miRNA screening in human pulmonary artery SMCs (HPASMC).
Bar graph showing the changes in the percentage (%) of Edu-positive cells (Edu+) after mimic-based overexpression of miRNAs vs miR-CTRL. As the log fold change for miR-34a-3p overexpression was – infinite; we used an arbitrary value of -10 for plotting.

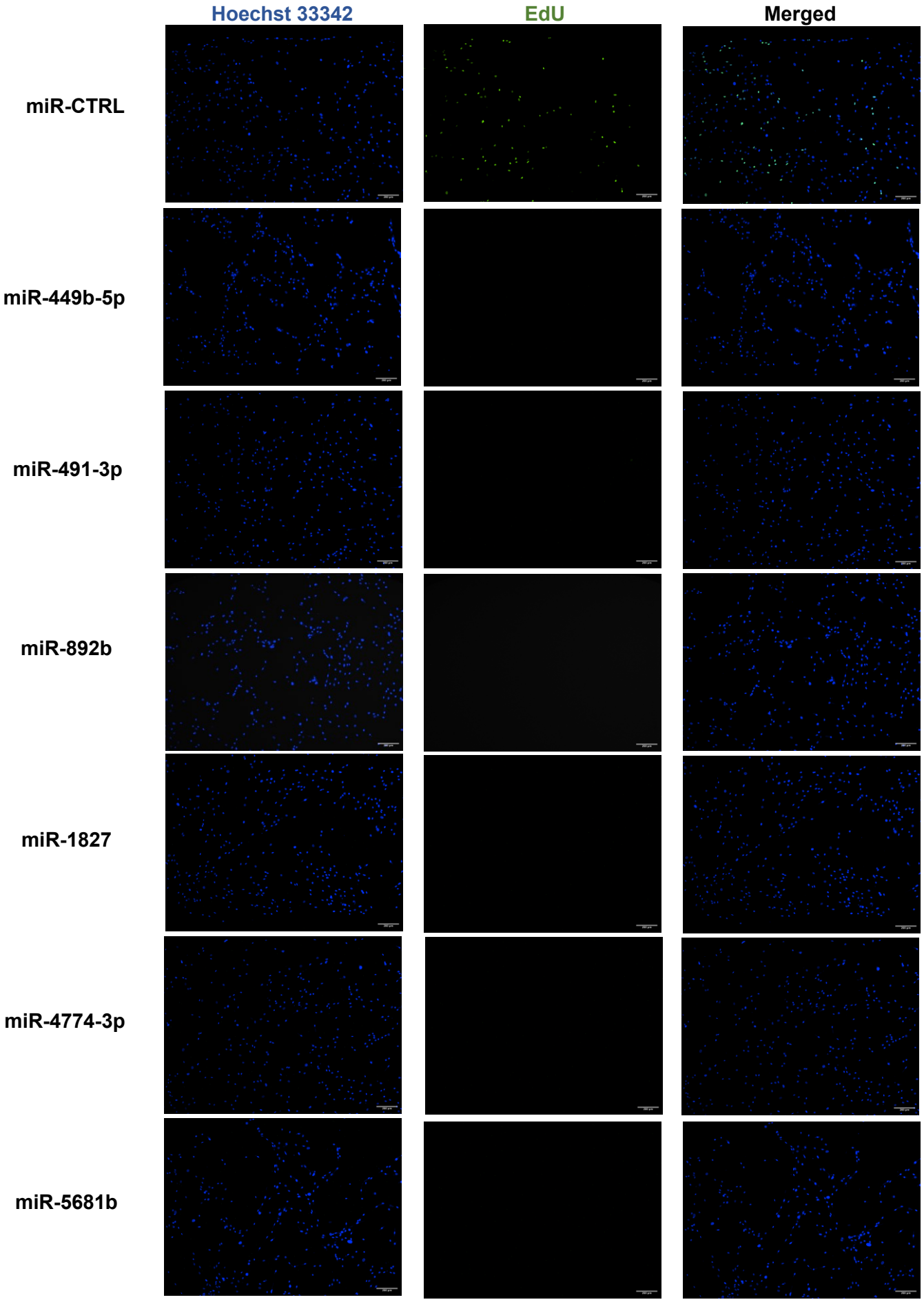

Figure S2. Representative images of human HPASMCs stained with Hoechst 33342 (blue) and EdU (green) following treatment with miR-CTRL or mimics for miR-449b-5p, miR-491-3p, miR-892b, miR-1827, miR-4774-3p and miR-5681b. Scale bar is 100μm.

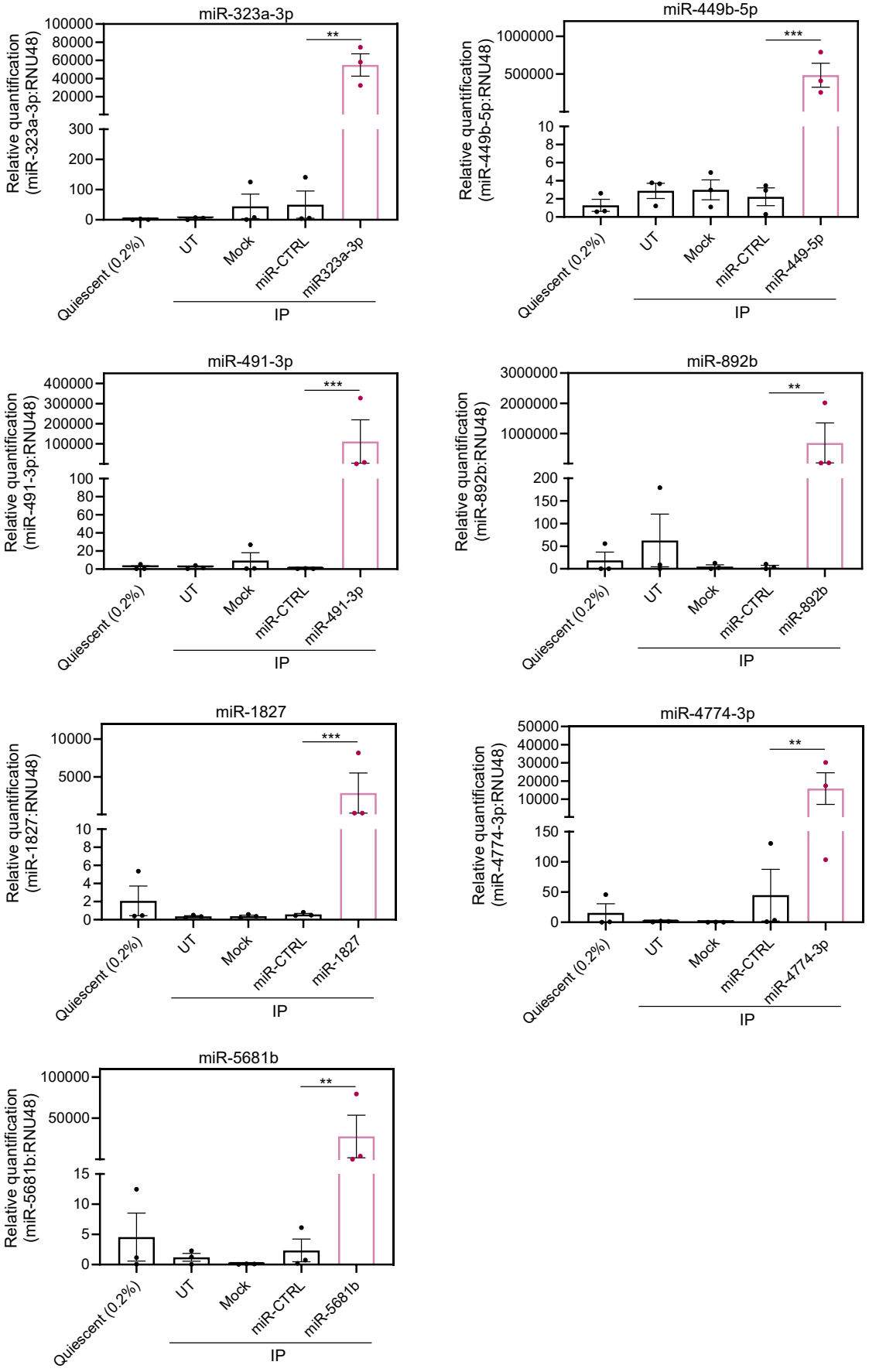

Figure S3: Confirmation of miRNA overexpression using mimics for miRNA miR-323a-3p, miR-449b-5p, miR-491-3p, miR-892b, miR-1827, miR-4774-3p, miR5681b in HSVSMC by RT-qPCR (n=3). UT: Untransfected, IP: IL-1α+PDGF-BB. Mock corresponds to lipofectamine only.
Statistical analysis was performed using a repeated measures ANOVA. P-values for the comparison between miRNA mimic treatment and miR-CTRL treatment obtained after Dunnet's test for multiple corrections are included on the graphs: $*P < 0.05$, $**P < 0.01$, $***P < 0.001$. n numbers correspond to distinct biological replicates.

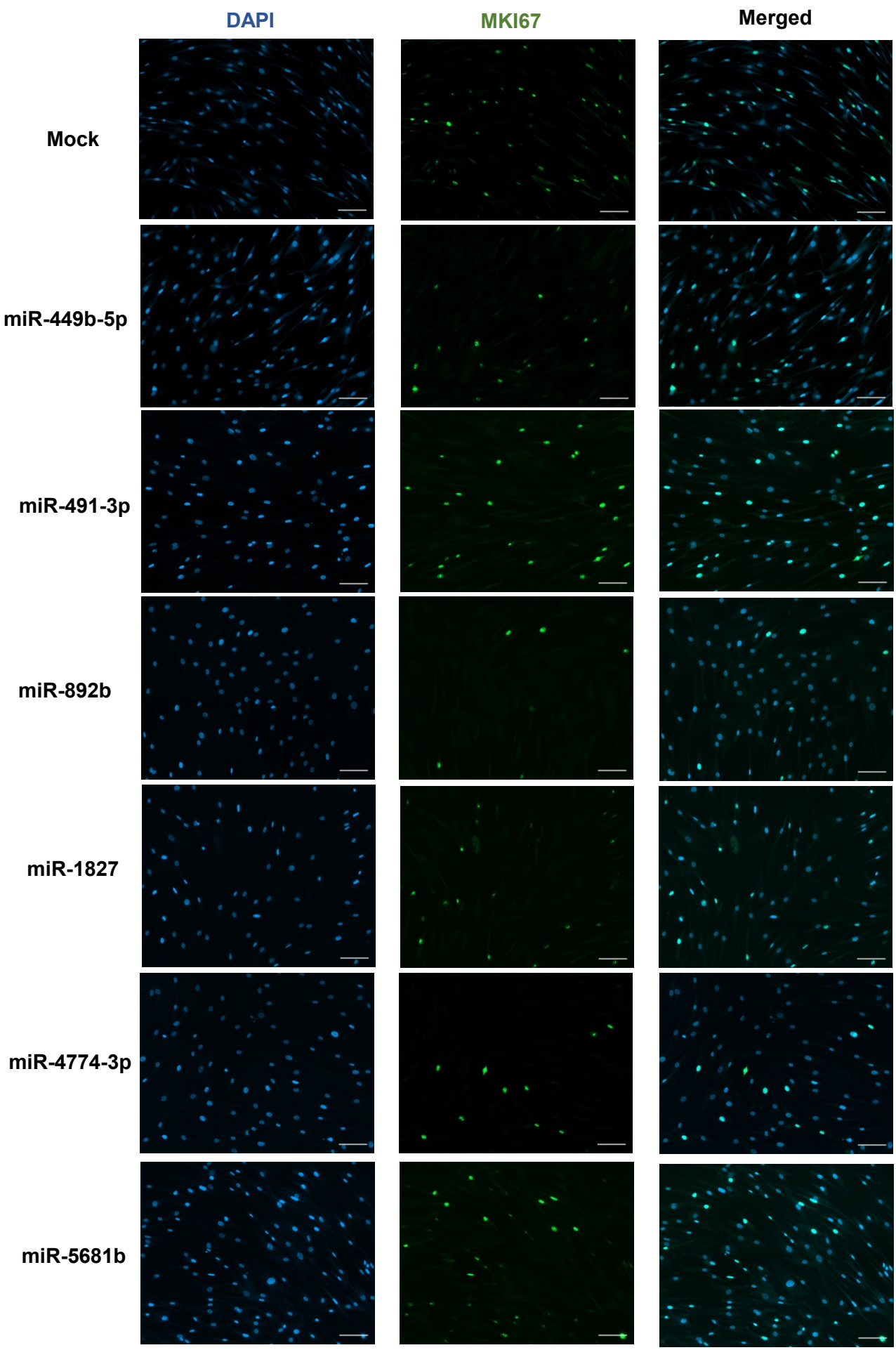

Figure S4: Representative images of MKI67 and DAPI staining of IL-1α/PDGF-BB-stimulated HSVSMCs transfected with mimic for miR-449b-5p, miR-491-3p, miR-892b, miR-1827, miR-4774-3p, miR5681b or Mock condition (lipofectamine only). Scale bar is 100μm.

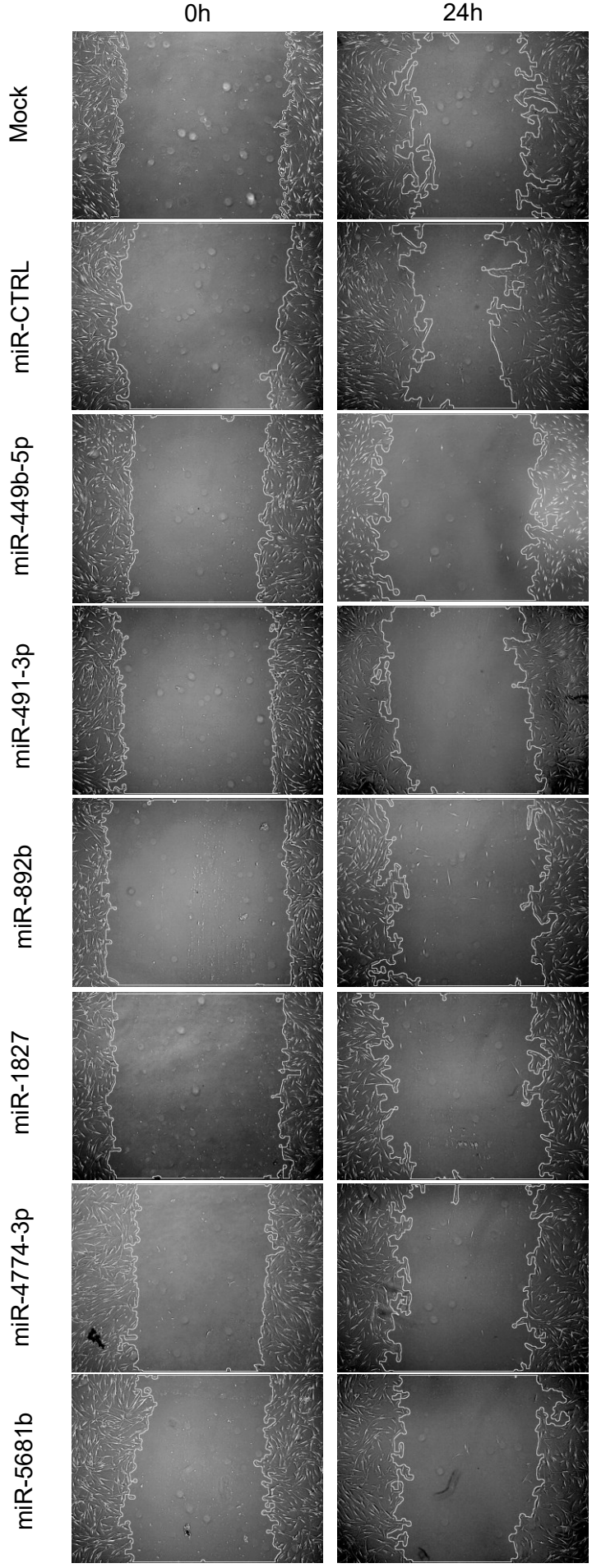

Figure S5: Wound healing assay of IL-1α/PDGF-BB-stimulated HSVSMCs transfected with the 7 miRNA mimics or miR-CTRL. Representative images from scratch assay at 0 and 24hours for miR-CTRL, miR-449b-5p, miR-491-3p, miR-892b, miR-1827, miR-4774-3p or miR-5681b. Scale bar is 500μm.

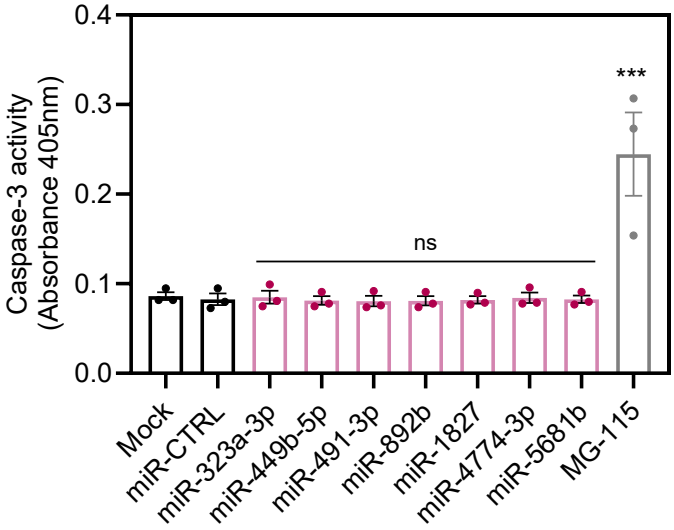

Figure S6: Quantification of Caspase-3 activity (absorbance measured at 405nm) in IL-1α/PDGF-BB -stimulated HSVSMCs transfected with the 7 miRNA mimics or miR-CTRL, as well as the "mock" transfection control (n=3). The proteasome inhibitor MG-115 was used as a positive control for apoptosis induction. Statistical analyses were done using Iman-Conover non-parametric ranking followed by repeated measures ANOVA. P-values for the comparison between miRNA mimic treatment and miR-CTRL treatment obtained after Dunnet's test for multiple corrections are included on the graph: ***$P < 0.001$, ns= non-significant. n numbers correspond to distinct biological replicates.

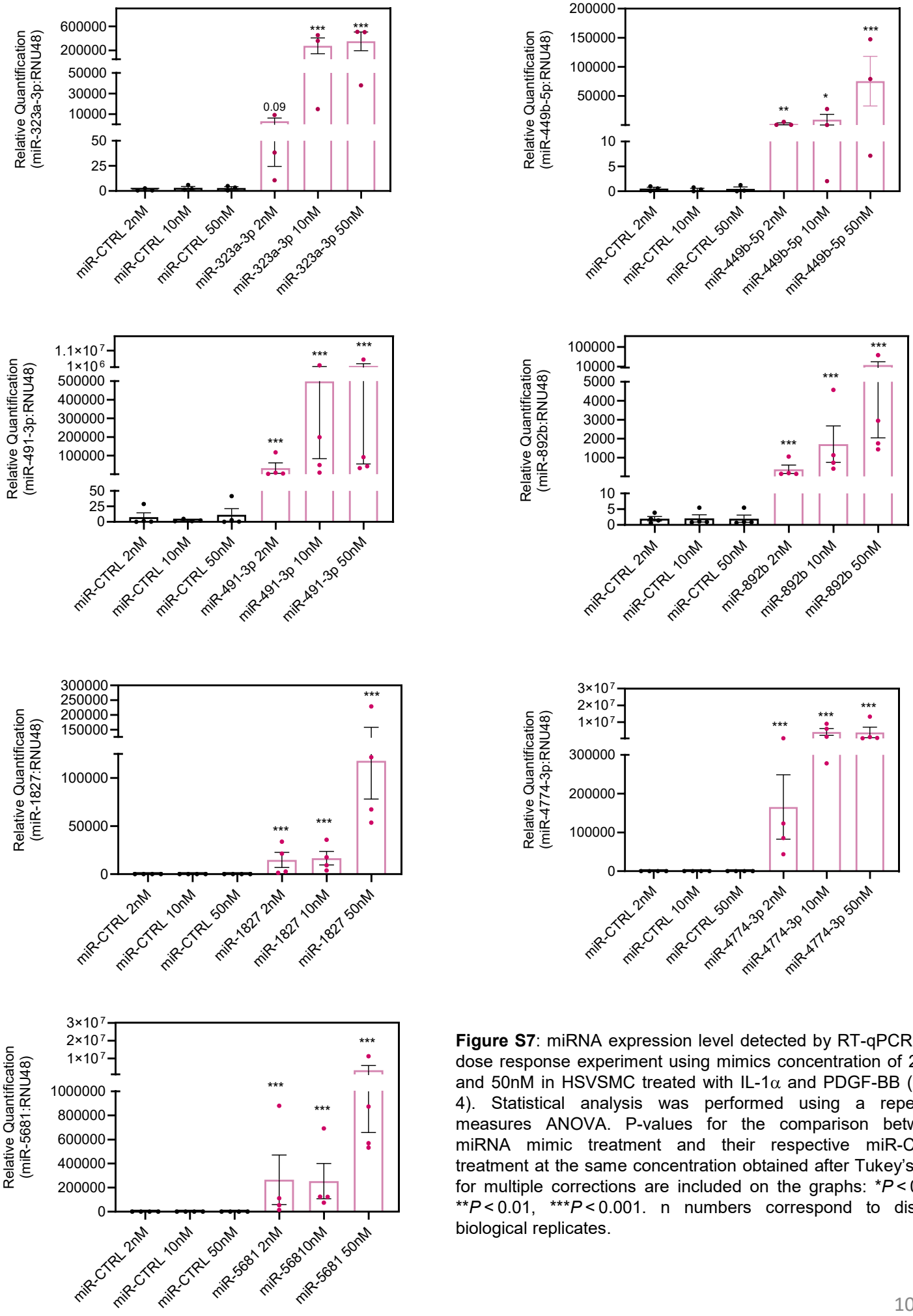

Figure S7: miRNA expression level detected by RT-qPCR in a dose response experiment using mimics concentration of 2, 10 and 50nM in HSVSMC treated with IL-1α and PDGF-BB (n=3-4). Statistical analysis was performed using a repeated measures ANOVA. P-values for the comparison between miRNA mimic treatment and their respective miR-CTRL treatment at the same concentration obtained after Tukey's test for multiple corrections are included on the graphs: $*P < 0.05$, $**P < 0.01$, $***P < 0.001$. n numbers correspond to distinct biological replicates.

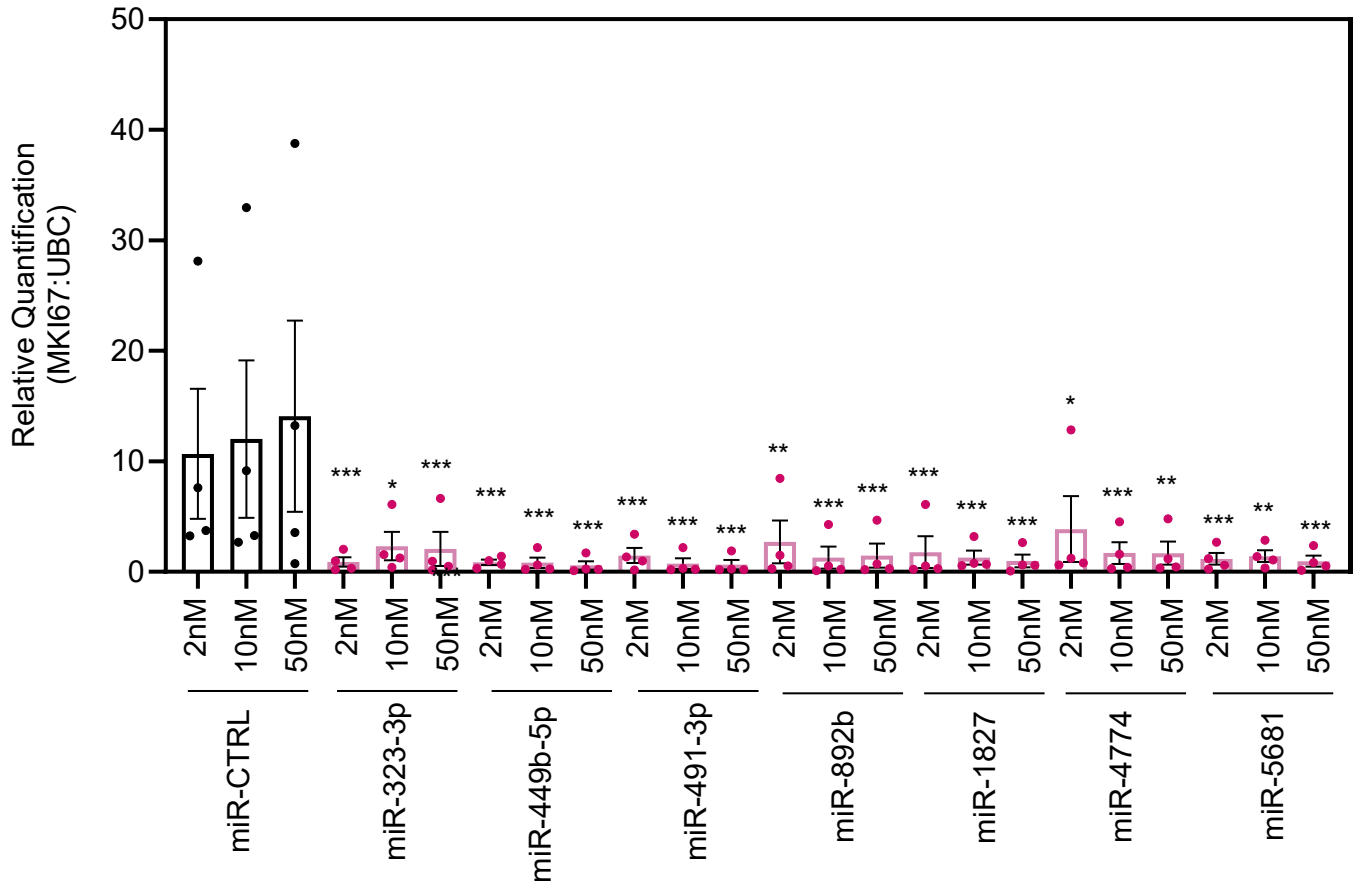

Figure S8: Effect of different doses of miRNA mimics on proliferation based on level of expression of MKI67 by RT-qPCR. HSVSMC were transfected with 3 different doses (2, 10 and 50nM) of mimics of the candidate miRNAs then treated with IL-1α and PDGF-BB (n=4). Statistical analysis was performed using a repeated measures ANOVA. P-values for the comparison between miRNA mimic treatment and their respective miR-CTRL treatment at the same concentration obtained after Tukey's test for multiple corrections are included on the graph: $*P < 0.05$, $**P < 0.01$, $***P < 0.001$. n numbers correspond to distinct biological replicates.

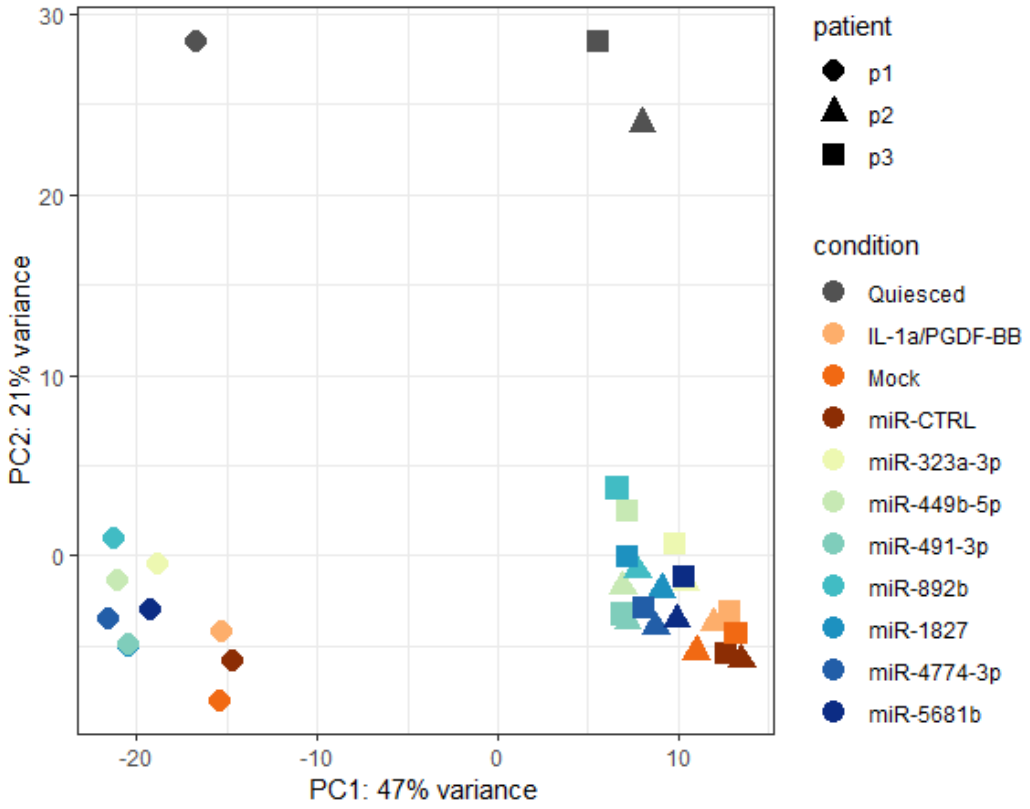

Figure S9: Principal component analysis plots of the HSVSMC RNAseq without removal of batch effect (removal of patient effect).

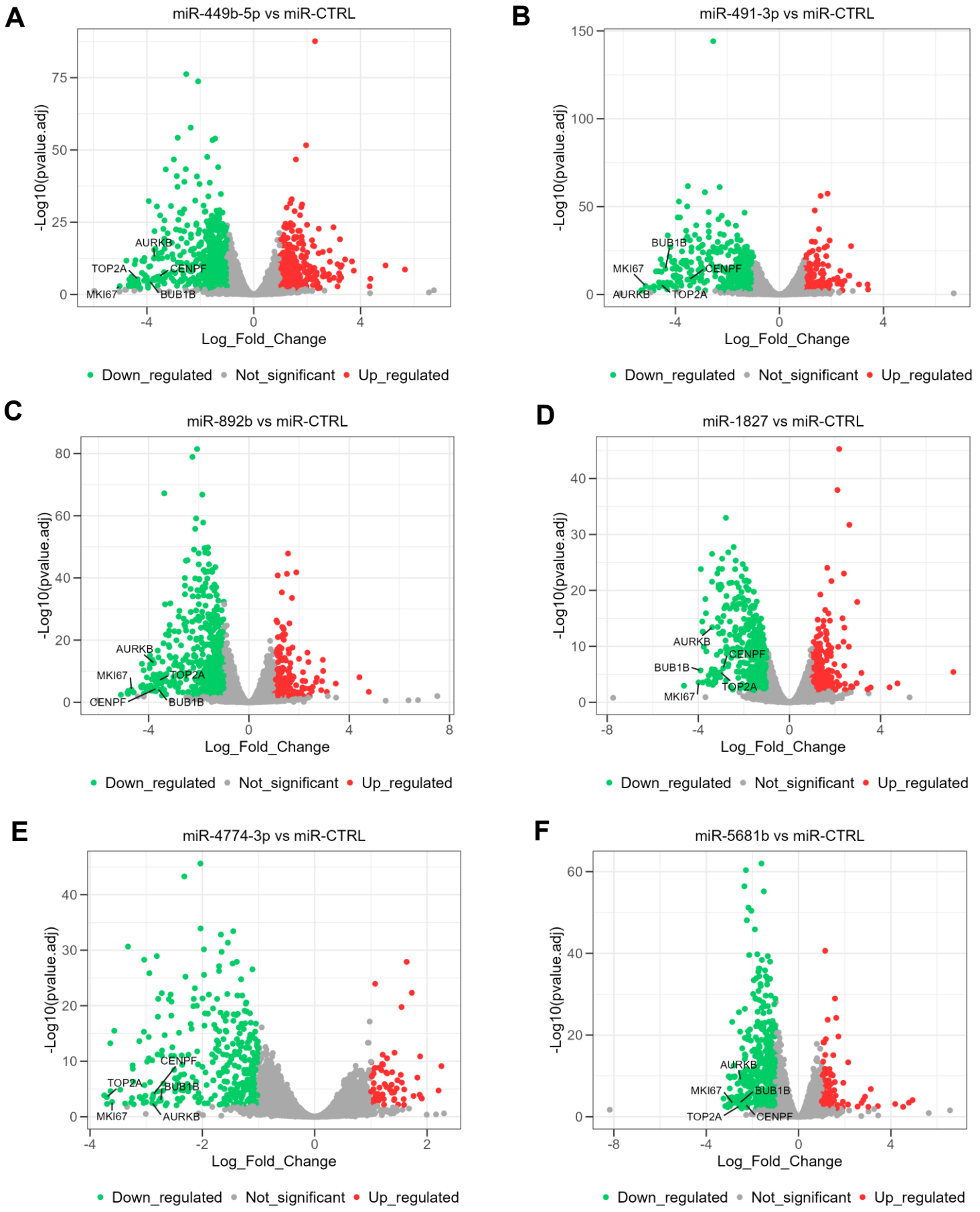

Figure S10: Volcano plot of the differentially expressed genes upon each miRNA overexpression (A) miR-449b-5p, (B) miR-491-3p, (C) miR-892b, (D) miR-1827, (E) miR-4774-3p and (F) miR-5681b . The comparisons were performed using DESeq2. Significant changes were identified using a threshold of absolute Fold Change >=2 and adjusted p value<0.01. Cell cycle genes MKI67, TOP2A, BUB1B, AURKB and CENPF are highlighted.

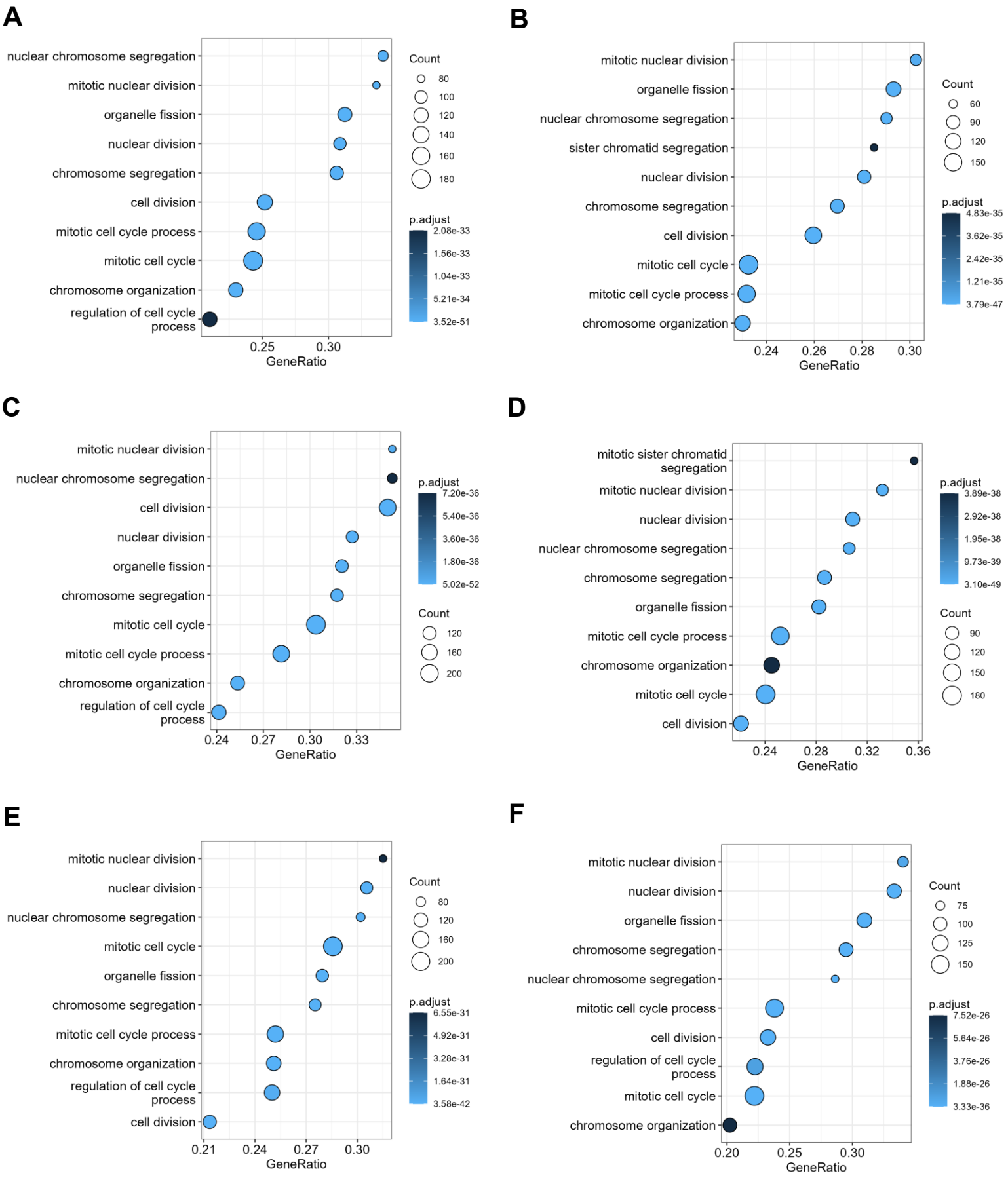

Figure S11: Top10 enriched Go Terms (Biological Process) based on gene set enrichment analysis for the genes differentially expressed upon (A) miR-449b-5p, (B) miR-491-3p, (C) miR-892b, (D) miR-1827, (E) miR-4774-3p and (F) miR-5681b overexpression.

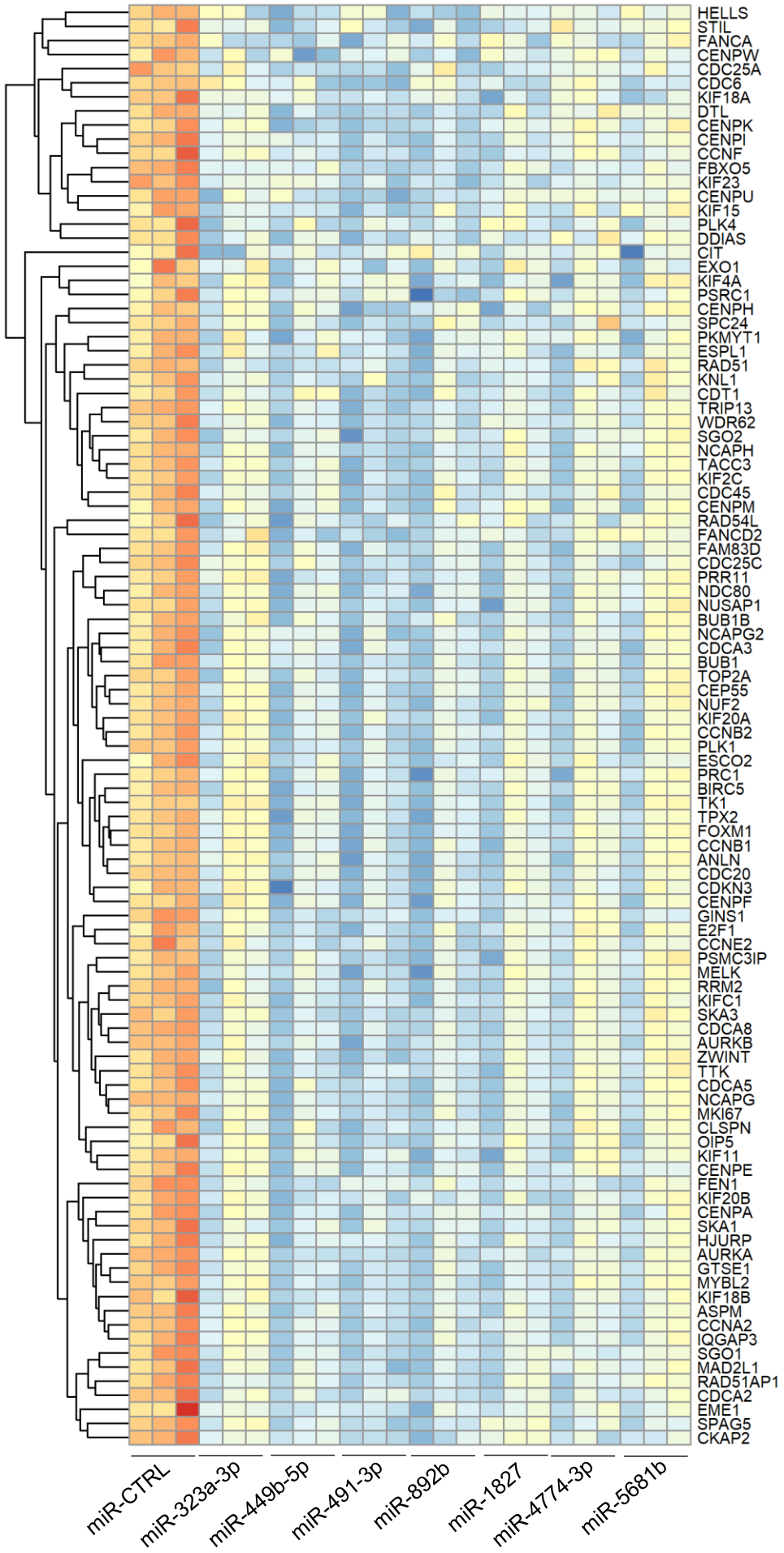

Figure S12: Heatmap of the 102 cell-cycle genes commonly down-regulated by all 7 mimics miRNAs in HSVSMC. Expression displayed as row z-score of Log2(FPKM+1)

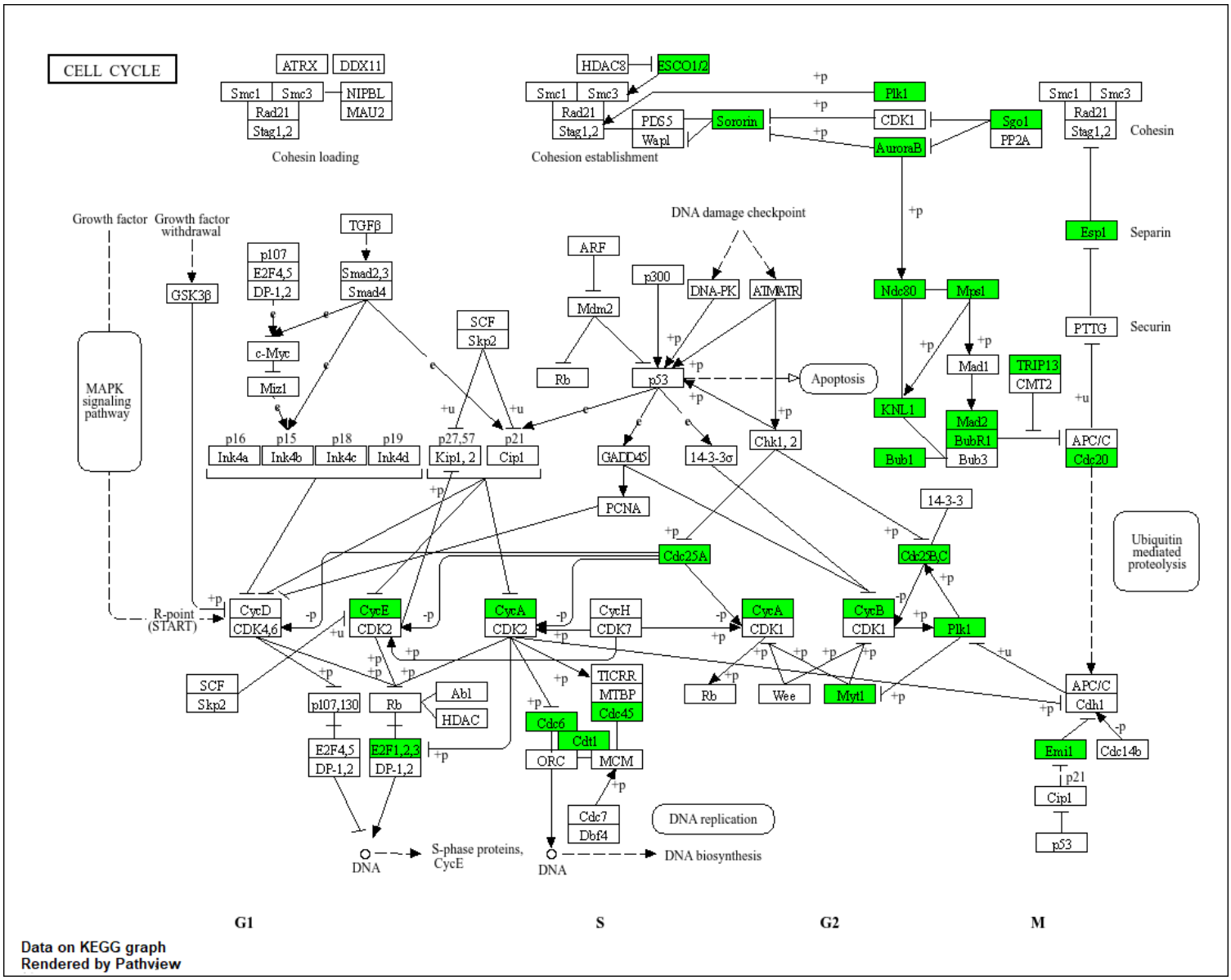

Figure S13: Diagram showing the genes regulated by all 7 miRNAs (in green) involved in cell cycle KEGG pathway (hsa04110) generated using Pathview.

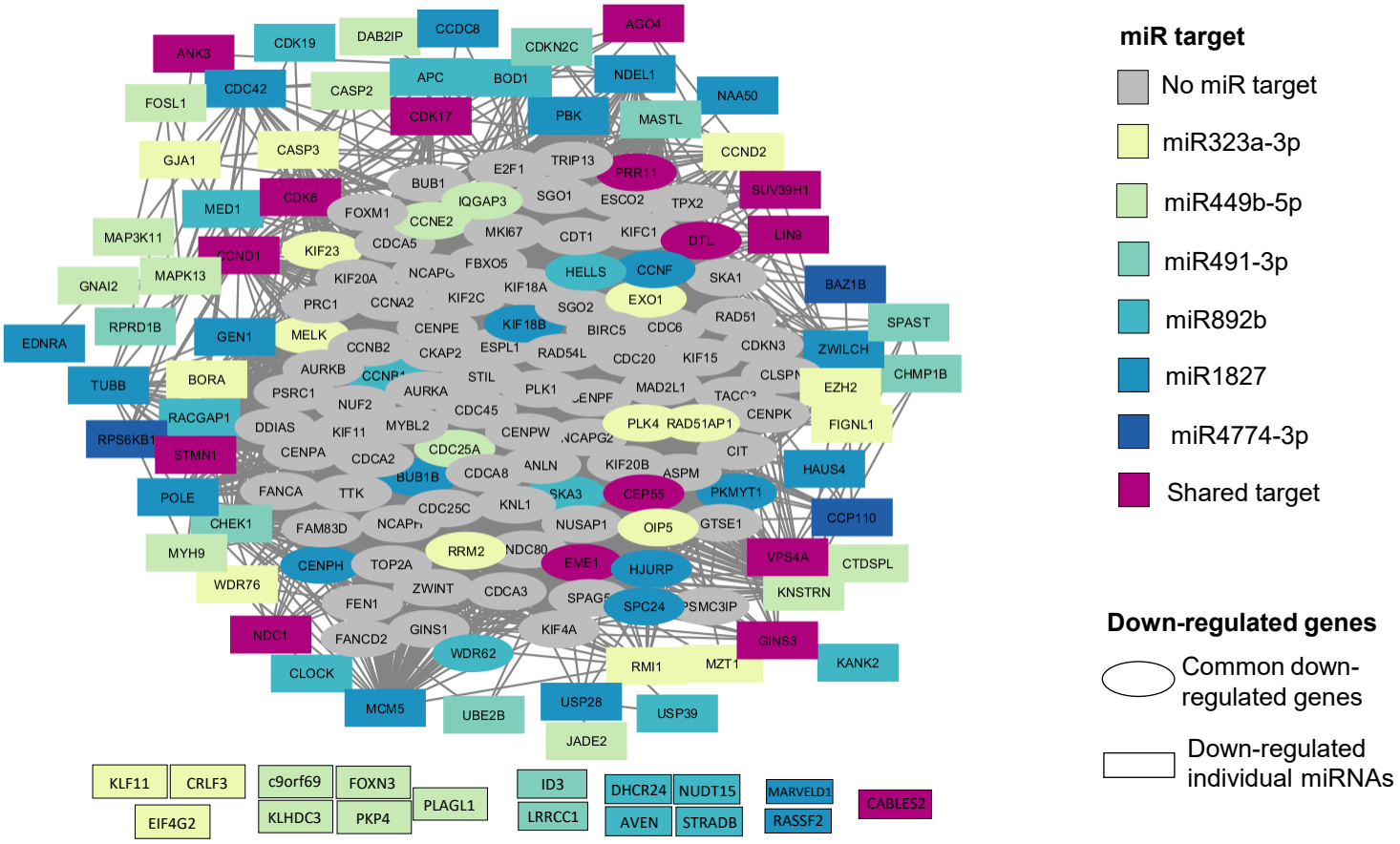

Figure S14: Network of candidate target genes and commonly down-regulated genes involved in Cell Cycle. The predicted gene interactions were obtained using STRING. The network was visualised using Cytoscape. The commonly down-regulated genes are represented in the centre of the network while the targets are located at the periphery.

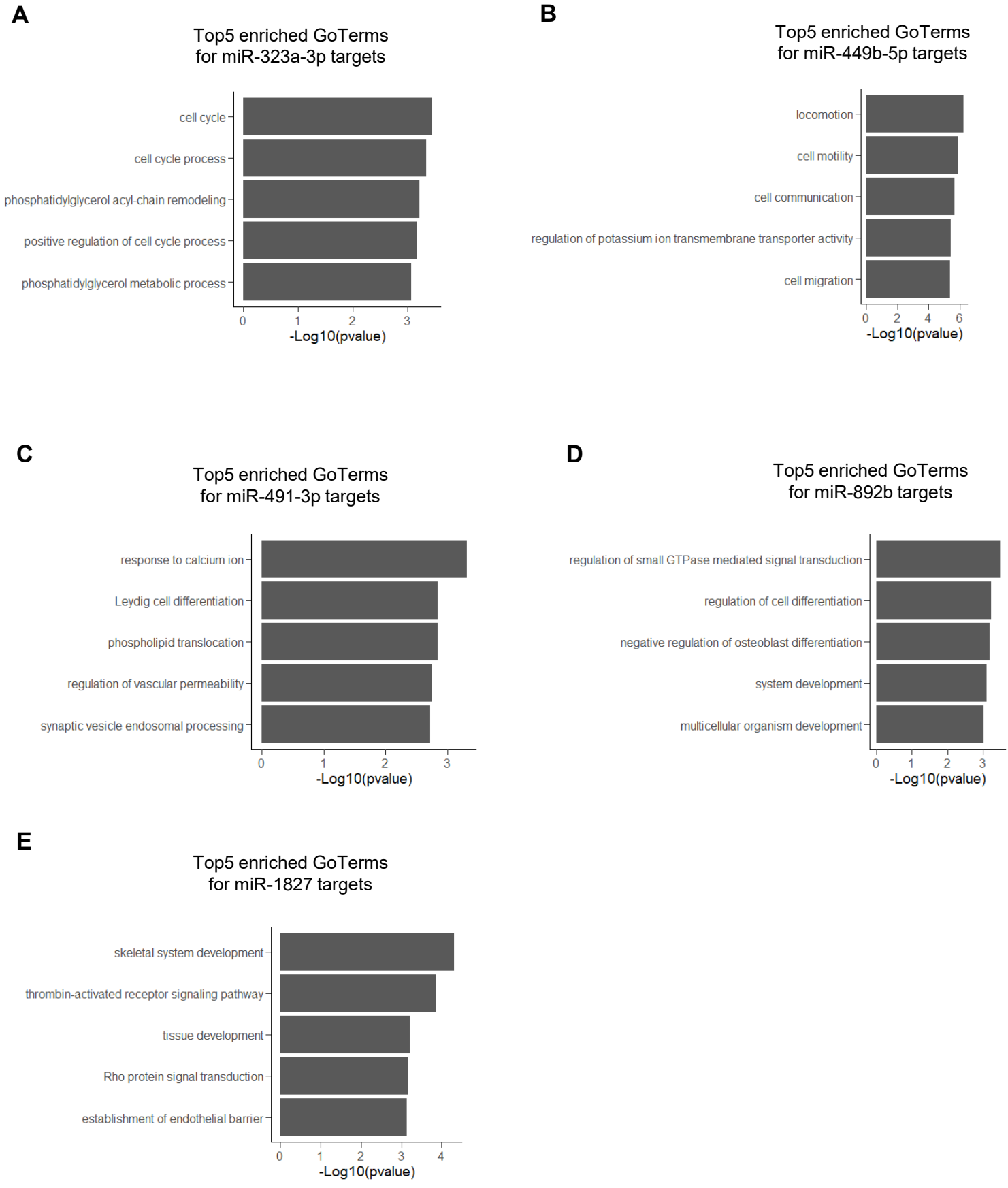

Figure S15: Top5 enriched GoTerns (Biological process) of miRNA candidate targets for (A) miR-323a-3p, (B) miR-449b-5p, (C) miR-491-3p, (D) miR-892b, (E) miR-1827.

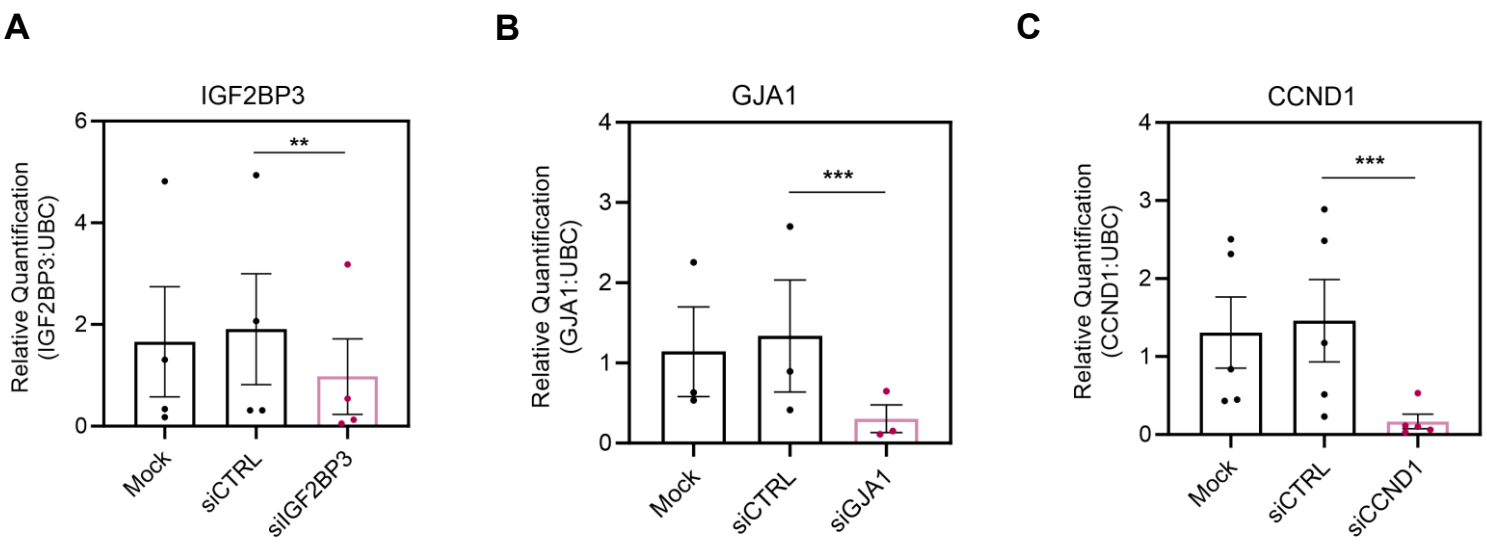

Figure S16: Knockdown validation of miRNA candidate target (A) IGF2BP3 (n=4), (B) GJA1 (n=3) and (C) CCND1 (n=5) in HSVSMC. Expression level was quantified by RT-qPCR after transfection with respective siRNA. Mock corresponds to Lipofectamine only.
Statistical analysis was performed using a repeated measures ANOVA. P-values for the comparison between siRNA target treatment and siRNA Control (siCTRL) obtained after Dunnet's test for multiple corrections are included on the graphs: $^{**}P < 0.01$, $^{***}P < 0.001$. n numbers correspond to distinct biological replicates.

A

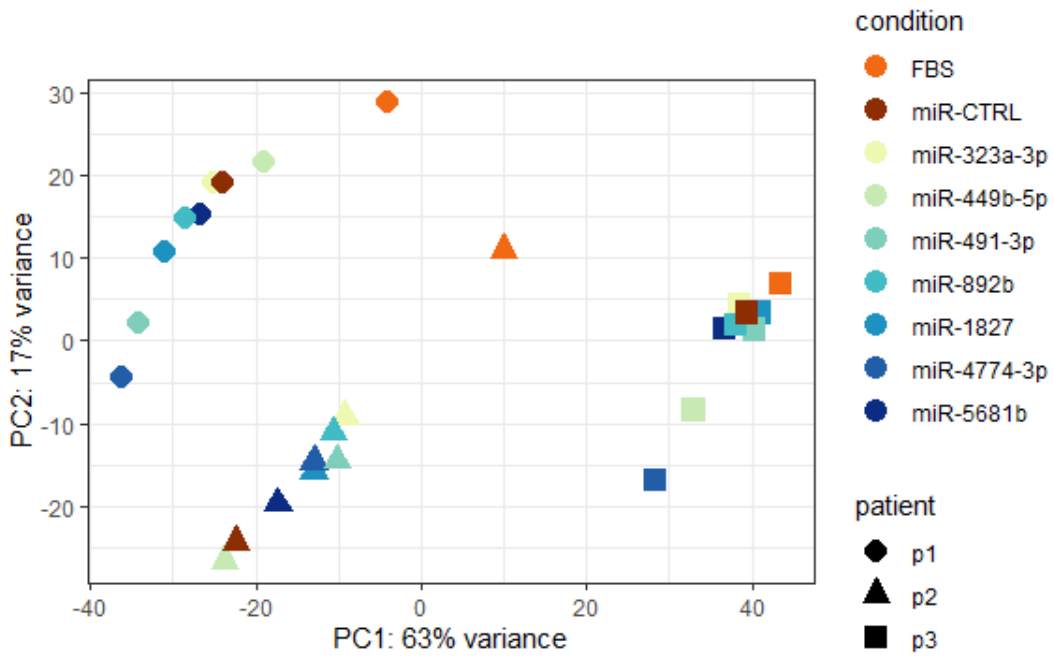

B

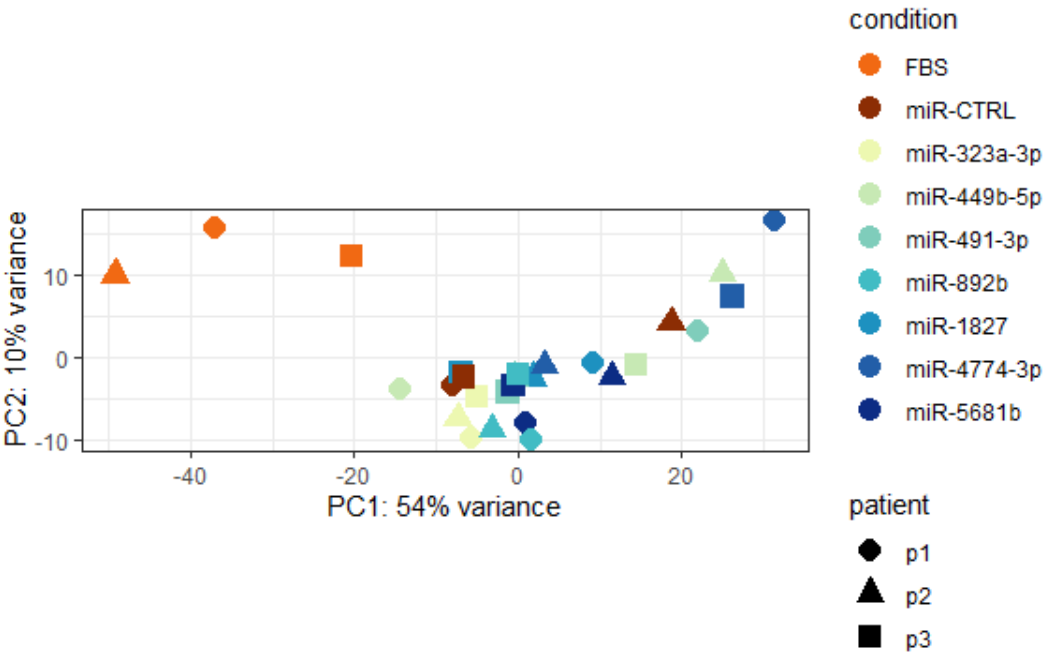

Figure S17: Principal component analysis plot of the HSVEC RNAseq without (A) and with (B) removal batch effect (removal of patient effect).

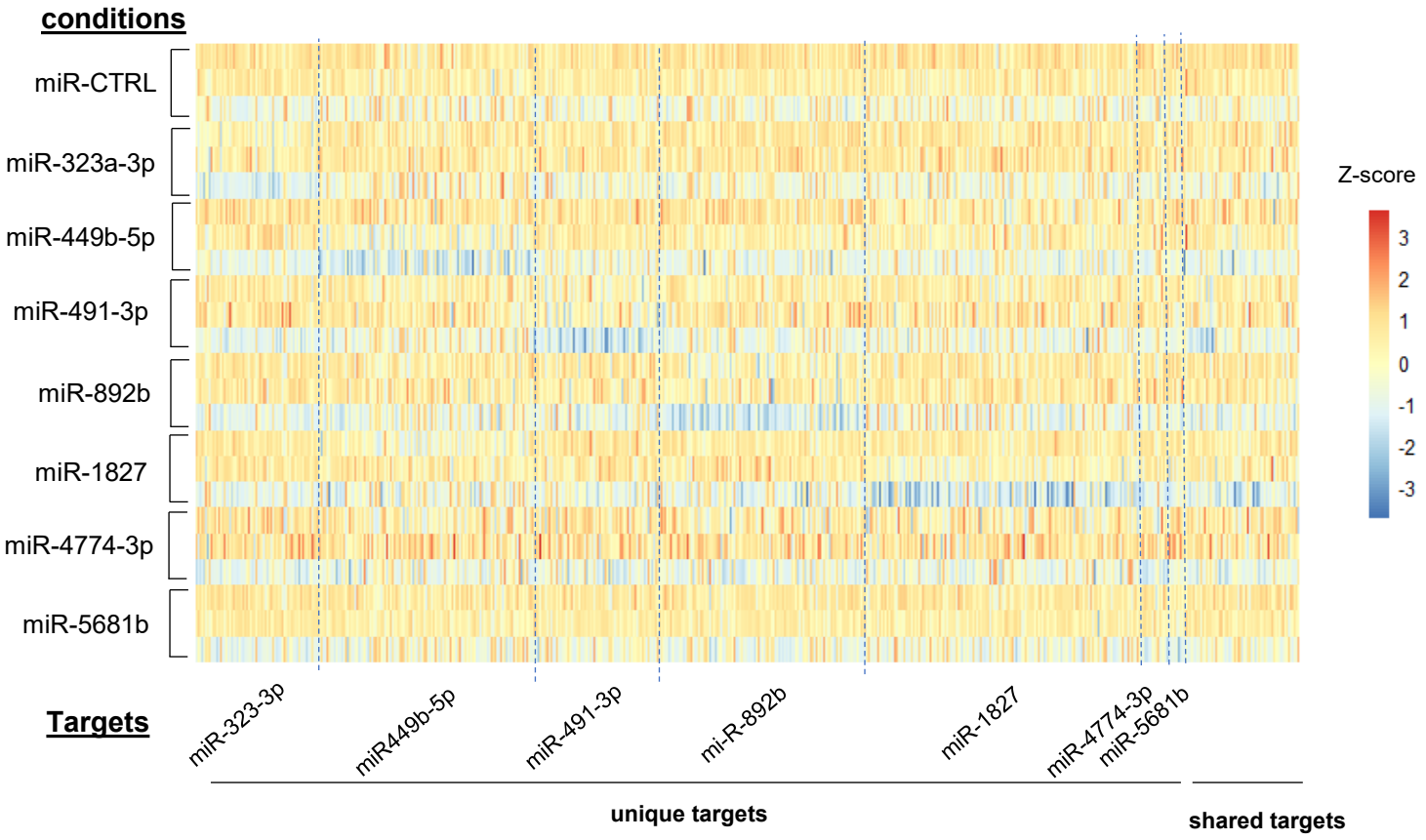

Figure S18: Heatmap showing the expression profile in HSVEC of all miRNA candidate targets identified in the HSVSMC RNAseq with a separation between unique and shared targets. Expression displayed as column z-score of Log2(FPKM+1).

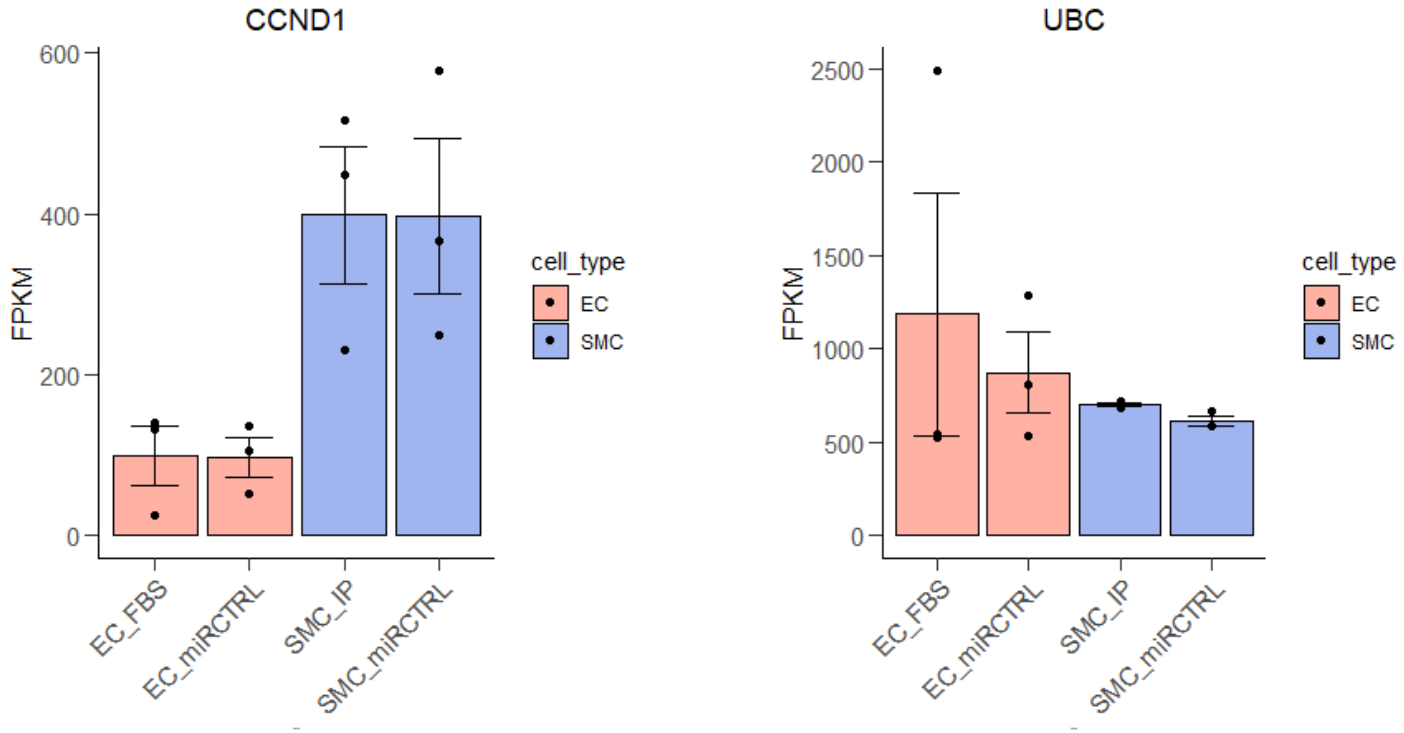

Figure S19: Expression level (as FPKM based on RNAseq) of CCND1 and UBC in HSVEC and HSVSMC under proliferative condition (FBS/IP) or with miR-CTRL treatment. IP: IL-1α+PDGF-BB treatment.

A

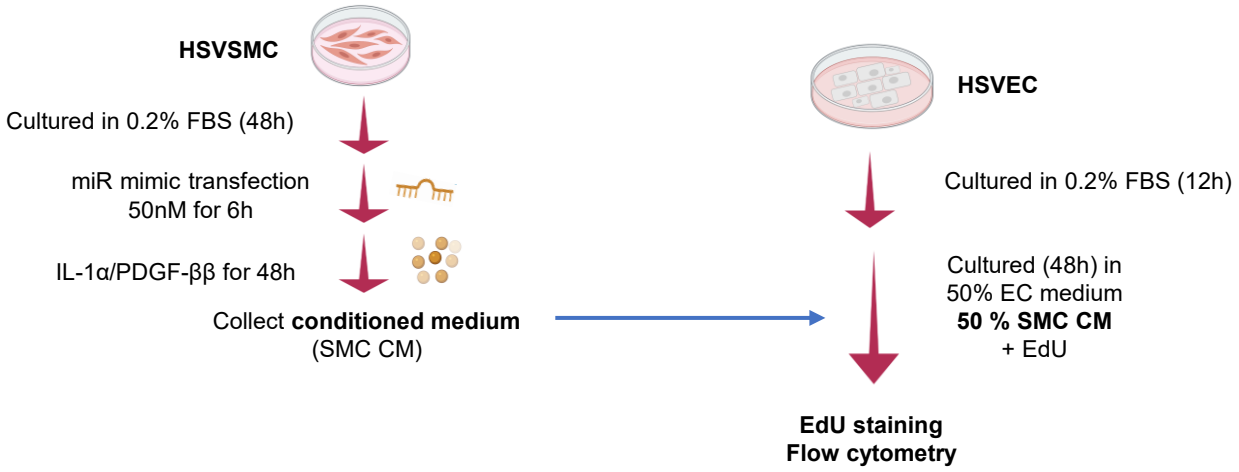

B

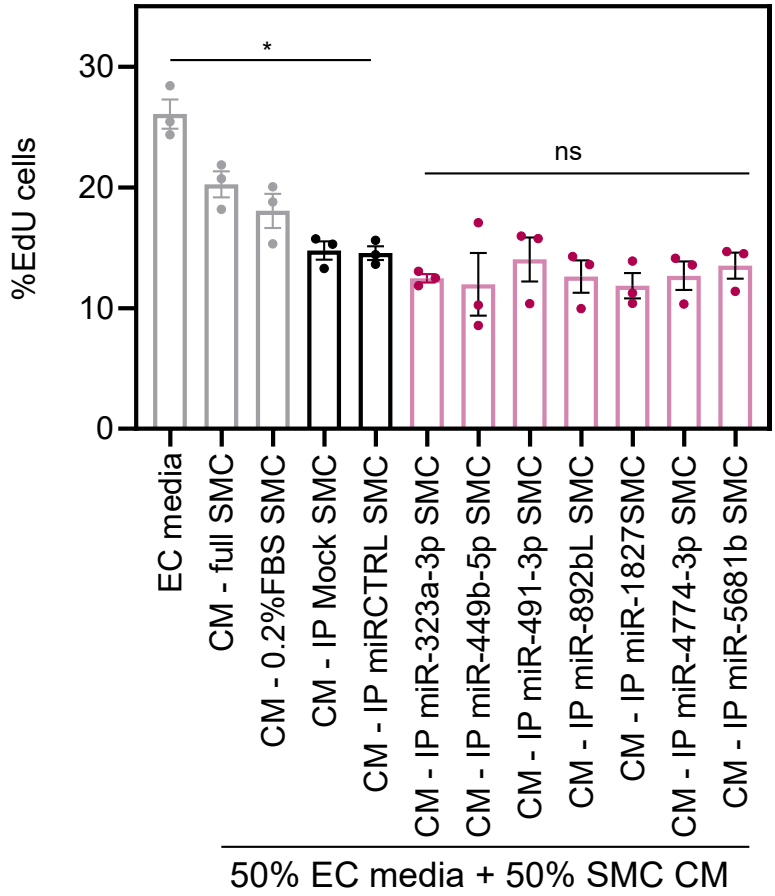

Figure S20: The overexpression of the candidate miRNA in HSVSMC does not lead to a negative paracrine effect on HSVEC proliferation *in-vitro*. (A) Schematic of the collection of conditioned media from HSVSMC treated with miR mimics and the treatment of HSVEC with the conditioned media. (B) Percentage of EdU+ HSVEC cells cultured with EC media or conditioned media from HSVSMC treated with miR-CTRL or indicated miR mimics.
IP: IL-1α+PDGF-BB. Mock: lipofectamine treated cells.

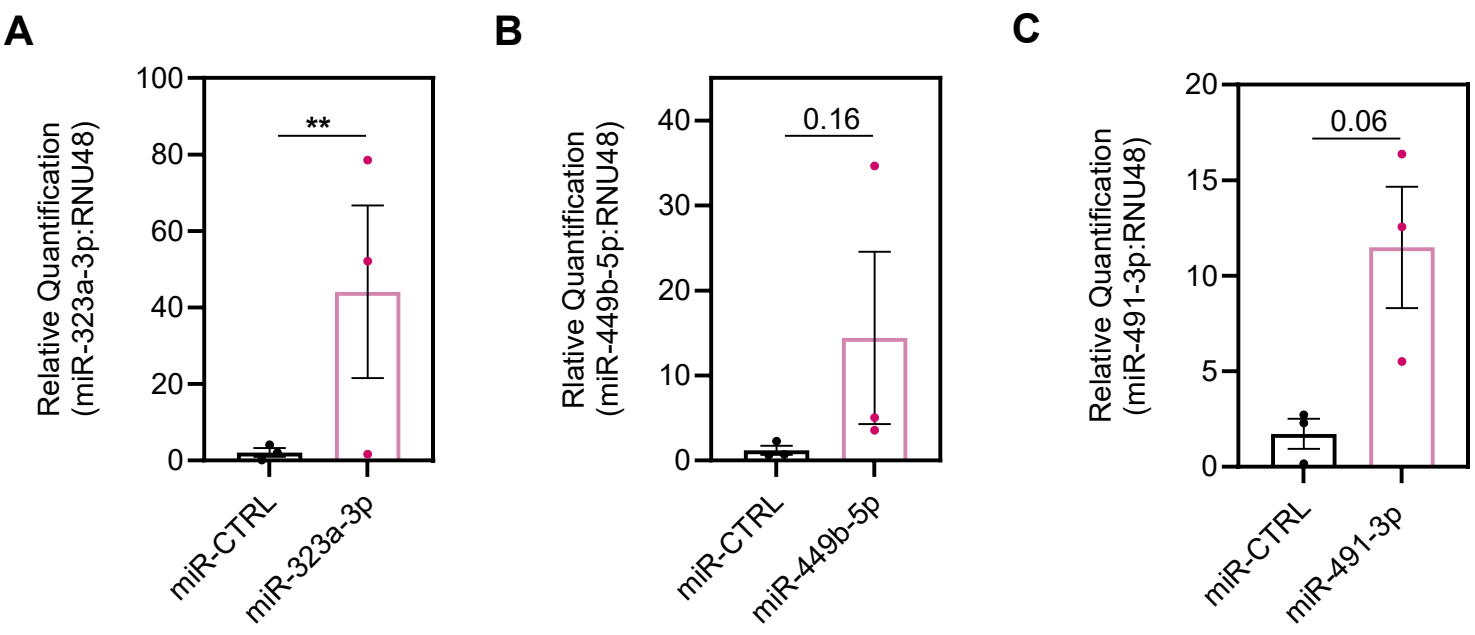

Figure S21: Quantification of (A) miR-323a-3p, (B) miR-449b-5p and (C) miR-491-3p expression level by RT-qPCR after transfection of mimics in the ex vivo vein organ model at 7 day time point (n=3).
Statistical analysis was performed using a paired t-test. P-values are included on the graphs: $^{**}P < 0.01$. n numbers correspond to distinct biological replicates.